

**TUMOR-INDUCED NEONEUROGENESIS
AND PERINEURAL TUMOR GROWTH:
A MATHEMATICAL APPROACH**

ARIANNA BIANCHI, KONSTANTINOS SYRIGOS, AND GEORGIOS LOLAS

(A.B.) DEPARTMENT OF MATHEMATICS AND MAXWELL INSTITUTE FOR MATHEMATICAL SCIENCES, HERIOT-WATT UNIVERSITY, EDINBURGH, SCOTLAND, EH14 4AS, UK

(K.S.) ONCOLOGY UNIT, 3RD DEPARTMENT OF INTERNAL MEDICINE, SOTIRIA GENERAL HOSPITAL, ATHENS SCHOOL OF MEDICINE, ATHENS, GREECE

(G.L.) CENTER FOR ADVANCING ELECTRONICS DRESDEN, TECHNISCHE UNIVERSITÄT DRESDEN, BARKHAUSEN BUILDING II/7B, 01062 DRESDEN, GERMANY

E-mail addresses: ab584@hw.ac.uk , ksyrigos@med.uoa.gr , georgioslolas@gmail.com.

Date: 2015.

ABSTRACT. Primary tumors infrequently lead to demise of cancer patients; instead, mortality and a significant degree of morbidity result from the growth of secondary tumors in distant organs (metastasis). It is well-known that malignant tumors induce the formation of a lymphatic and a blood vascular network around themselves. A similar but far less studied process occurs in relation to the nervous system and is referred to as *neoneurogenesis*; in fact, recent studies have demonstrated that tumors initiate their own innervation. However, the relationship between tumor progression and the nervous system is still poorly understood. This process is most likely regulated by a multitude of factors in the tumor-nerve microenvironment and it is therefore important to study the interactions between the nervous system and tumor cells through mathematical/computational modelling; this may reveal the most significant factors of the plethora of interacting elements regulating *neoneurogenesis*. The present work is a first attempt to model the neurobiological aspect of cancer development through a (simple) system of differential equations. The model confirms the experimental observations that a tumor is able to promote nerve formation/elongation around itself, and that high levels of nerve growth factor (NGF) and axon guidance molecules (AGMs) are recorded in the presence of a tumor. Our results also reflect the observation that high stress levels (represented by higher norepinephrine release by sympathetic nerves) contribute to tumor development and spread, indicating a mutually beneficial relationship between tumor cells and neurons. The model predictions suggest novel therapeutic strategies, aimed at blocking the stress effects on tumor growth and dissemination.

Significance Statement. The major strength of the article resides in its novelty: it constitutes a first attempt to model tumor-induced *neoneurogenesis* through a set of differential equations. The mathematical model presented is simple; nevertheless, it gives some interesting insights of the process. In particular, it shows that a tumor is able to induce high nerve density around itself and cause higher levels of NGF and AGMs in the tissues. Furthermore, the model confirms the empirical observation that stress (correlated with increased release of norepinephrine) affects tumor progression. The model suggests that cancer-induced *neoneurogenesis* is a decisive component of tumor progression and metastasis. In this regard, we envision that tumor-nerve interactions could represent a therapeutic target of primary significance. It is hoped this work will inspire further theoretical investigation into tumor *neoneurogenesis*. Also, we hope that experiments will follow to investigate proposed hypotheses such as the inverse dependence of tumor growth and progression on stress modulators (through an Allee effect).

1. INTRODUCTION

A relationship between tumors and the nervous system has been suspected since the second century AD with the work of the Greek physician Galen [83]. Traditionally, the nervous system has not been considered to be actively involved in the process of metastasis. However, recent studies have demonstrated the presence of neurons in peritumoral regions of several human tumors, and the number of tumor-associated neurons has been correlated with metastases [2, 51]. The relative importance of pre-existing versus newly-formed neurons to metastasis is not understood. Although pre-existing peritumoral neurons are likely to be sufficient for tumor spread, recruitment of neurons into the close proximity of a tumor may increase the propensity of tumors to metastasize. Increased nerve density and/or presence of intratumoral neurons should be regarded as an additional pathway for metastasis.

Significant progress has also been made in understanding the effects of stress- and depression-mediated release of chemicals by the nervous system on tumor cell dissemination [1, 52, 87]. On the one hand tumor cells produce factors that induce the formation of a neural network, and on the other the newly formed nerves release neurotransmitters that affect tumor growth and migration [46, 54]. Following the terminology suggested in [29], the formation of new nerve branches is herein called *neoneurogenesis*, in analogy to lymphangiogenesis and (blood) angiogenesis.

The present model aims to investigate how solid tumors induce peripheral nerve proliferation and how different types of nerves affect tumor growth and metastasis by releasing substances such as neurotransmitters. Also, we address the question of which role stress plays in cancer progression. This model was mainly inspired by recent works presented in [2, 54], focussing predominantly on prostate cancer [80]. The study in [2] combines *in vitro* experiments with autopsy analysis of prostate cancer patients; in [54] the authors explore the effects of the nervous system on tumor progression by altering nerve structure and receptor activity in mice, after implanting human tumor cells in the animals. Since the scope of our work does not include tumorigenesis, our model simulations start with a nonzero initial condition for primary tumor cells, reflecting the tumor cells implanation described in [54]. Our aim is to investigate the further evolution of these cells and their interactions with the preexisting prostate-surrounding nerves. The model takes major inspiration from [2], supporting the hypothesis of a symbiosis between nerves and tumor cells.

2. BIOLOGICAL BACKGROUND

2.1. Neurons, neurotransmitters and the Autonomic Nervous System (ANS). Neurons (or *nerve cells*) are the core components of

the nervous system. The electrical signals travelling inside a neuron are converted into signals transmitted by certain chemicals (*neurotransmitters*); these are then passed to another neuron across a *synapse*. A neurotransmitter released by a nerve binds to a receptor on another cell and, according to the receptor type, induces a certain action. The collection of all the neuronal structures that together control body functions below the level of consciousness (for instance, heart and respiratory rate, digestion and pupillary dilation) constitute the ANS. The ANS is in turn made of three sub-systems; here we will focus only on two of them: the Sympathetic Nervous System (SNS, also called “fight or flight” system), which is responsible for quick response processes, and the Parasympathetic Nervous System (PNS, also known as “rest and digest” system), which governs slower responses such as gastro-intestinal functions.

2.2. Tumor-induced neurogenesis. Tumors induce innervation around themselves [30, 51, 65] and, in general, high levels of innervation in tumors correlate with a poor disease outcome [2, 54]. Tumor cells have the ability to produce substances, such as Nerve Growth Factor (NGF), that stimulate the growth and improve the survival of nerve cells [20, 35, 73]. NGF also promotes tumor growth [20] and inhibits aggregation of cancer cells and thus enhances tumor invasion, although this process is currently poorly understood [21].

Tumors also release Axon Guidance Molecules (AGMs). These molecules were originally considered only for their role in the nervous system as guidance cues for axons.¹ In recent years, however, it was shown that many AGMs can also influence neuronal survival and migration and likely play an important role in cancer progression [56]. There are at least three different families of AGMs (semaphorins, slits and netrins), which seem to have different roles in nervous system development and cancer progression. They are found in many different body tissues and can regulate cell migration and apoptosis (for a review of the role of AGMs in cancers, see [11]).

2.3. ANS effects on tumor progression. It was originally believed that the nervous system only indirectly affected cancer development, through perineural invasion (that is, the spread of tumors along nerve fibers [28, 86]) and modulation of the immune function [87]. Indeed, neurotransmitters regulate the cytotoxicity of T lymphocytes and natural killer cells [47] and induce leukocyte migration [27, 46]; the consequent immunosuppression can favor tumor growth and progression, impairing the anti-tumor response [4, 87]. However, it is the migratory

¹The term *axon guidance* denotes the process by which neurons send out axons along a precise path in order to reach the correct targets. The tip of an axon (or *growth cone*) is equipped with receptors that can sense (gradients of) chemicals, called *guidance cues*, which “tell” them where to expand [19].

effect of neurotransmitters that first suggested a *direct* link between nerves and tumor progression. One theory for the spread of metastases from a primary tumor to a certain organ claims that circulating cancer cells are attracted and settle in a specific region of the body due to the presence of factors such as chemokines or AGMs [11, 50]. This assumption is in agreement with the well-known “seed and soil” hypothesis [33]. In particular, several studies have shown that neurotransmitters influence the migratory activity of cancer cells, perhaps by inducing a phenotypic change towards a more motile phenotype via intracellular signalling [30, 63], or simply by chemotaxis [22]. In addition, some neurotransmitters also induce tumor growth [46]. Indeed, tumor cells express many receptors, including serpentine receptors [26] to which neurotransmitters are ligands. Neurotransmitters can induce several behavioral changes in tumor cells, mostly increasing their proliferation and/or migration (a summary of such effects can be found in [46]).

3. MATHEMATICAL MODEL

We define the *main domain* of our study as a portion of the body containing the prostate and its near surroundings, thus including both the tumor and the neighboring nerves. All the variables, with the exception of the migrating tumor cells (see below), are average concentrations/densities over this domain, which vary in time. We develop a compartmental model in which an *extra domain* is considered for the tumor cells which leave the main domain. A schematic of the model, showing the variables and their interactions, can be found in Figure 1.

We distinguish between *primary* tumor cells (T_p) and *migrating* tumor cells (T_m). The former are those that constitute the original tumor mass; when they detach and leave the orthotopic site of the tumor they are then designated migrating. The migrating cells are particularly dangerous because they have the potential to form metastases. Herein we do not explicitly account for the further development of the migrated tumor cells: our variable T_m represents an indication of *potential* metastasis formation.

NGF (G) is a neurotrophin (a kind of protein) which stimulates the growth and enhances the survival of both Sympathetic Nerve Cells (SNCs) and Parasympathetic Nerve Cells (PNCs). It has been found to be secreted by tumor cells. AGMs (A) also affect the survival and moreover the growth of both SNCs and PNCs. In reality, there are many kinds of AGMs, which can have completely different effects on nerve and tumor development. Here, for simplicity, we consider them as a single variable; taking into account the different types of AGMs would be one step towards improving the model in future.

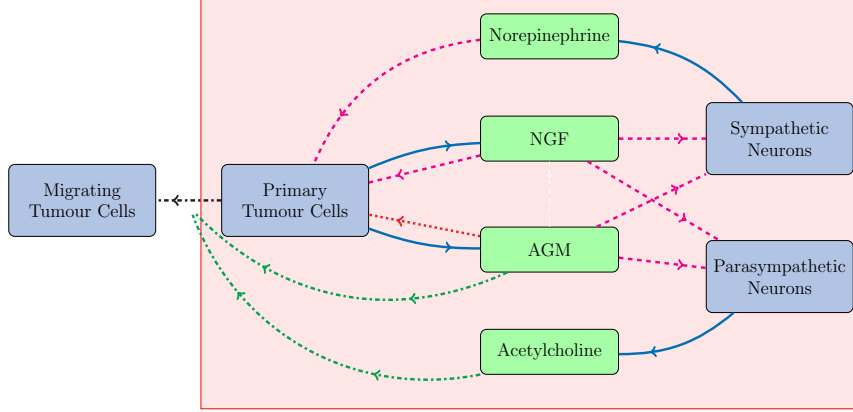


FIGURE 1. A schematic representation of the interactions among the model variables. Each variable corresponds to a rounded-corners rectangular box; note that cells are in **BLUE** while chemicals are in **GREEN**. The light red-shaded rectangular area represents the main domain, that is the prostate and its immediate surroundings. Concerning the arrows, **solid blue** denotes production, **dashed magenta** denotes enhancement of growth and/or survival (and axonal extension in the case of neurons), **dash-dotted green** denotes migration enhancement, **dash-dotted black** actual migration and **dotted red** denotes apoptosis induction.

The growth of both SNCs (S) and PNCs (P) is enhanced by NGF and AGMs. In addition, both types of nerve cell respond to a neurotransmitter called *acetylcholine* (N_a), but only PNCs produce it; SNCs instead secrete *epinephrine* (also known as *adrenaline*) and *norepinephrine* (N_n , also called *noradrenaline*). Furthermore, norepinephrine enhances tumor cell survival, growth and chemotaxis whereas acetylcholine seems to stimulate tumor cell invasion and migration [54].

3.1. Model equations. It is well documented that tumor cells naturally undergo mitosis. The model accounts for this by taking constant growth rates r_T and r_{T_m} for primary and migrating tumor cells, respectively. Only a fraction of primary tumor cells exhibit proliferation; this is due to the presence of a necrotic core, that we assume to be defined by the half inner radius of the (spherical) tumor mass [5]. This assumption leads to the conclusion that only 7/8 of the tumor volume (and thus primary tumor cells) proliferate. Primary tumor cells are also exposed to the chemicals present in the domain which influence the tumor development. Since tumor growth is enhanced by NGF [93], we assume that the growth rate of T_p is increased in a saturating manner by this factor. It has been shown that a classic logistic equation

is often not suitable for modelling tumor growth [43]. Here we include an Allee effect² in the growth term to take into account the fact that tumor cell populations tend to die out at low densities. This effect is traditionally found in ecological literature; its inclusion in cancer modelling was already suggested in [43]. The use of ecological concepts in cancer biology and modelling is a promising development in tumor research [68]. Here we take the *Allee threshold*, as defined in [43], to be a function $\vartheta = \vartheta(N_n)$ that decreases as the norepinephrine level increases. This choice reflects the observation that norepinephrine enhances tumor cell survival [25, 78]. Tumor cells also die at a constant rate d_T . Interestingly, some AGMs (such as netrin-1) are also thought to control tumor cell apoptosis [48, 84]; we model this phenomenon by adding a linear dependence on A to the death term. Finally, another relevant aspect of tumor cell dynamics is migration. Tumor cells can spontaneously disaggregate and move away from their original site [69]. This process is enhanced by substances produced by nerve cells and distant organs, including AGMs [8] and acetylcholine [27, 46]. Hence, the densities of primary and migrated tumor cells are described by the following equations:

$$\begin{aligned} \frac{dT_p}{dt} = & \underbrace{\frac{7}{8}T_p \cdot \left(r_T + \frac{G}{\tau_1 + \tau_2 G}\right)}_{\text{growth upregulated by NGF}} \cdot \underbrace{\left(1 - \frac{T_p}{k_T}\right) \cdot \left(\frac{T_p}{\vartheta(N_n)} - 1\right)}_{\text{logistic growth with Allee effect}} \\ & - \underbrace{d_T(1 + \delta A) \cdot T_p}_{\text{cell death increased by AGM}} - \underbrace{(\mu_0 + \mu_1 A + \mu_2 N_a) \cdot T_p}_{\text{migration induced by AGM and acetylcholine}}, \end{aligned} \quad (1)$$

$$\frac{dT_m}{dt} = \underbrace{(r_{T_m} - d_T) \cdot T_m}_{\text{natural cell growth/death}} + \underbrace{(\mu_0 + \mu_1 A + \mu_2 N_a) \cdot T_p}_{\text{tumor cell migration from the primary tumor}}, \quad (2)$$

where³

$$\vartheta(N_n) = \frac{\theta_1}{1 + \theta_2 N_n}.$$

We are interested in the effects that tumor-secreted NGF and AGMs have on the system; here the tumor secretion rate of these two growth factors is assumed to be constant [29, 30]. We do not include other sources of NGF and AGMs in the main domain since these have a negligible effect on the dynamics that we want to study here (their effect on nerve growth in absence of tumor is implicitly included in the logistic growth of nerve cells – see below). As chemicals, both NGF and AGMs decay at constant rate d_G and d_A , respectively. They are also internalized by both tumor [71] and nerve cells [14], which bind

²The *Allee effect* is an ecological term describing a correlation between the size and the per capita growth rate of a population.

³See Appendix A.3 for the motivation of the definition of $\vartheta(N_n)$.

them to their surface receptors. Here we assume that SNCs and PNCs bind the proteins at the same rate (namely, γ_2 for NGF and γ_4 for AGM). The evolution equations describing NGF and AGM dynamics in the domain are therefore given by

$$\frac{dG}{dt} = \underbrace{s_G T_p}_{\text{production by tumor cells}} - \underbrace{d_G G}_{\text{decay}} - \underbrace{[\gamma_1 T_p + \gamma_2 (S + P)] G}_{\text{internalization by tumor and nerve cells}}, \quad (3)$$

$$\frac{dA}{dt} = \underbrace{s_A T_p}_{\text{production by tumor cells}} - \underbrace{d_A A}_{\text{decay}} - \underbrace{[\gamma_3 T_p + \gamma_4 (S + P)] A}_{\text{internalization by tumor and nerve cells}}. \quad (4)$$

We assume that in a normal (i.e. tumor-free) setting both SNCs and PNCs grow in a logistic manner and tend to their carrying capacities k_S and k_P , which are equal to their normal equilibrium values. However, when tumor cells are present nerve growth is enhanced by the secreted NGF [49, 53] and AGMs [88]. This additional growth is modelled by two saturating functions and is not subject to logistic limitation. This is due to the fact that, given the complex shape of neurons, it is difficult to estimate an actual maximum density. Nerve growth can also occur as axon elongation, which does not take a significant portion of space. Thus, the equations characterizing SNC and PNC rate of change are

$$\frac{dS}{dt} = \underbrace{r_S \left(1 - \frac{S}{k_S}\right) \cdot S}_{\text{logistic growth and remodelling}} + \underbrace{\left(\frac{G}{\sigma_1 + \sigma_2 G} + \frac{A}{\sigma_3 + \sigma_4 A}\right) \cdot S}_{\text{extra growth upregulated by NGF and AGM}}, \quad (5)$$

$$\frac{dP}{dt} = \underbrace{r_P \left(1 - \frac{P}{k_P}\right) \cdot P}_{\text{logistic growth and remodelling}} + \underbrace{\left(\frac{G}{\pi_1 + \pi_2 G} + \frac{A}{\pi_3 + \pi_4 A}\right) \cdot P}_{\text{extra growth upregulated by NGF and AGM}}. \quad (6)$$

Norepinephrine and acetylcholine are produced by SNCs and PNCs, respectively, [37] at respective net rates s_n and s_a that we assume to be constant. However, these two neurotransmitters are also released by other cell types [57, 90] and we include constant sources c_n , c_a in their equations. As chemicals, they decay at constant rates d_n and d_a , respectively. Finally, they are absorbed by tumor cells [46, 54] at constant rates γ_5 and γ_6 , respectively. The evolution equations for the

neurotransmitters are then expressed by

$$\frac{dN_n}{dt} = \underbrace{c_n}_{\text{const. source}} + \underbrace{s_n S}_{\text{production by SNCs}} - \underbrace{d_n N_n}_{\text{decay}} - \underbrace{\gamma_5 T_p N_n}_{\text{uptake by tumor cells}}, \quad (7)$$

$$\frac{dN_a}{dt} = \underbrace{c_a}_{\text{const. source}} + \underbrace{s_a P}_{\text{production by PNCs}} - \underbrace{d_a N_a}_{\text{decay}} - \underbrace{\gamma_6 T_p N_a}_{\text{uptake by tumor cells}}. \quad (8)$$

3.2. Parameters and initial conditions.

Parameters. Table 1 reports a list of all the parameters appearing in the model equations. Each parameter is supplied with its estimated value, units and source used (when possible) to assess it. References in brackets mean that although the parameter was not *directly* estimated from a dataset, its calculated value was inspired by the biological literature. When no data were found to inform a parameter value, this was taken to be of the same order of magnitude of another reasonably similar one. A detailed description of the estimation of each parameter can be found in Appendix A.

Initial conditions. In order to explore model predictions in different scenarios we will run simulations under different initial conditions on the primary tumor cells. In particular, $T_0^{20\%}$ and $T_0^{10\%}$ denote an initial density of primary tumor cells corresponding to 20% and 10% of the prostate volume, respectively (see Appendix A.2 for details). A relatively high percentage is used due to the fact that data concerning the tumor-nerve system evolution are only available for late stages of tumor progression (as in [2]). We assume that the initial amount of tumor cells have been implanted in healthy individuals (as done in [54], although there human tumor cells were implanted in mice). We also assume zero initial conditions for T_m , NGF and AGMs, because we are interested in the growth factors produced by the tumor (see above section). All the other values are assumed to be at their normal (tumor-free) level when the model simulation starts.

The initial values are listed in Table 2.

4. RESULTS

A simulation of the system of equations (1)–(8) with initial primary tumor cell density $T_0^{20\%}$ (see above) is shown in Figure 2, where the MatLab function `ode45` was used to obtain the approximate solutions. Overall, the output is in good *qualitative* agreement with the experimental observations associated with aggressive human prostate tumor as reported in [2]. Both sympathetic and parasympathetic nerves are, in the presence of tumor, significantly increased in the region around

PARAMETER	VALUE	UNITS	SOURCE
r_T	4.81×10^{-4}	day^{-1}	[75]
r_{T_m}	1×10^{-4}	day^{-1}	estimated $\approx r_T$
τ_1	307.4	$\text{pg day (mm}^3)^{-1}$	[93]
τ_2	22.7	day	[93]
k_T	10^6	$\text{cells (mm}^3)^{-1}$	([66])
θ_1	10^4	$\text{cells (mm}^3)^{-1}$	estimated $\approx 1\%$ of k_T
θ_2	1	$\text{mm}^3 \text{pg}^{-1}$	([12])
d_T	1.27×10^{-2}	day^{-1}	[18]
δ	1.29×10^{-2}	$\text{mm}^3 \text{pg}^{-1}$	[10]
μ_0	0.22	day^{-1}	[69]
μ_1	9.8×10^{-6}	$\text{mm}^3 \text{pg}^{-1} \text{day}^{-1}$	[38]
μ_2	2×10^{-3}	$\text{mm}^3 \text{pg}^{-1} \text{day}^{-1}$	[54]
s_G	2.22×10^{-3}	$\text{pg cell}^{-1} \text{day}^{-1}$	[20]
d_G	22.18	day^{-1}	[81]
γ_1	5.57×10^{-5}	$\text{mm}^3 \text{cell}^{-1} \text{day}^{-1}$	[71]
γ_2	5×10^{-2}	$\text{mm}^3 \text{cell}^{-1} \text{day}^{-1}$	[14]
s_A	5.06×10^{-3}	$\text{pg cell}^{-1} \text{day}^{-1}$	[42]
d_A	2.4	day^{-1}	[77]
γ_3	10^{-5}	$\text{mm}^3 \text{cell}^{-1} \text{day}^{-1}$	estimated $\approx \gamma_4$
γ_4	1.47×10^{-5}	$\text{mm}^3 \text{cell}^{-1} \text{day}^{-1}$	[41]
r_S	6×10^{-2}	day^{-1}	[20]
k_S	0.26	$\text{cells (mm}^3)^{-1}$	[54]
σ_1	1.29×10^2	$\text{pg day (mm}^3)^{-1}$	[17, 74]
σ_2	50	day	[17, 74]
σ_3	7.79	$\text{pg day (mm}^3)^{-1}$	[44]
σ_4	0.01	day	([44])
r_P	7	day^{-1}	[16, 17]
k_P	0.03	$\text{cells (mm}^3)^{-1}$	[54]
π_1	0.33	$\text{pg cell}^{-1} \text{day}^{-1}$	[17]
π_2	0.1	day	([17])
π_3	1	$\text{pg day (mm}^3)^{-1}$	estimated $\approx \sigma_3$
π_4	0.01	day	estimated $\approx \sigma_4$
c_n	5×10^2	$\text{pg (mm}^3)^{-1} \text{day}^{-1}$	([82])
s_n	1.6	$\text{pg cells}^{-1} \text{day}^{-1}$	[31]
d_n	1.66	day^{-1}	[82]
γ_5	2×10^{-3}	$\text{mm}^3 \text{cell}^{-1} \text{day}^{-1}$	[40]
c_a	2.65×10^4	$\text{pg (mm}^3)^{-1} \text{day}^{-1}$	([61])
s_a	0.73	day^{-1}	[67]
d_a	49.91	day^{-1}	[6]
γ_6	10^{-3}	$\text{mm}^3 \text{cell}^{-1} \text{day}^{-1}$	estimated $\approx \gamma_5$

TABLE 1. A list of all the parameters appearing in the model equations.

the prostate, and the number of tumor cells leaving the domain are constantly increasing, matching the metastases-formation report in [2, 54].

INIT.VALUE	VALUE	UNITS	SOURCE
$T_p(0)$	$T_0^{20\%}, T_0^{10\%}$	cells/mm ³	calculated
$T_m(0)$	0	cells/mm ³	assumption
$G(0)$	0	pg/mm ³	assumption
$A(0)$	0	pg/mm ³	assumption
$S(0)$	0.26	cells/mm ³	[54]
$P(0)$	0.03	cells/mm ³	[54]
$N_n(0)$	3×10^2	pg/mm ³	[82]
$N_a(0)$	5.3×10^2	pg/mm ³	[61]

TABLE 2. Values of the model variables at $t = 0$.

Concerning the primary tumor mass, our model predicts that after an initial increase it reaches a nonzero equilibrium; this is in agreement with the results of [54], which reports an increase in tumor mass within the prostate. Also the fact that NGF and AGM levels stay high seems realistic: NGF levels are higher in inflammation [89] and some studies report that semaphorin 7A and netrin-1 levels are significantly elevated in patients subject to chemotherapy and some kinds of cancers, respectively [39, 72]. Neurotransmitters reduce rapidly to a low nonzero level following the sudden implantation of tumor cells. On the other hand, our results are not in *quantitative* agreement with [54]; in particular, the present model reaches an equilibrium approximately 5 days after tumor cells implantation, whilst in [54] it takes weeks to observe such significant changes. This may be due to the fact that the model does not take into account other elements of the prostate environment (such as lymphatic and blood vasculature) which compete with the nervous system for growth factors and space, thus potentially slowing down the dynamics. This observation is relevant, since it implies that more elements surrounding the tumor site need to be considered in order to model tumor development more precisely.

An interesting feature of the model is that a smaller initial condition for primary tumor cells, for instance $T_0^{10\%}$, gives rise to completely different dynamics. In this case the primary tumor goes to zero after few days, while migrating tumor cells initially increase but then decrease to zero (Figure 3). This behavior is in accordance with the hypothesis that a tumor cell colony has to be bigger than a certain threshold in order to proliferate [43]. Note that the migrated tumor cells could cause tumor development in another site of the body where the conditions are more favorable. It is notable that the model is able to reflect this strong dependence of tumor progression on its initial conditions; this appears to be an important feature in modern cancer research inspired by ecological dynamics [43]. Our Allee threshold, lying between $T_0^{10\%}$ and $T_0^{20\%}$, appears to be unrealistically high but, to the authors' knowledge, no measurement of this parameter is available for comparison. In

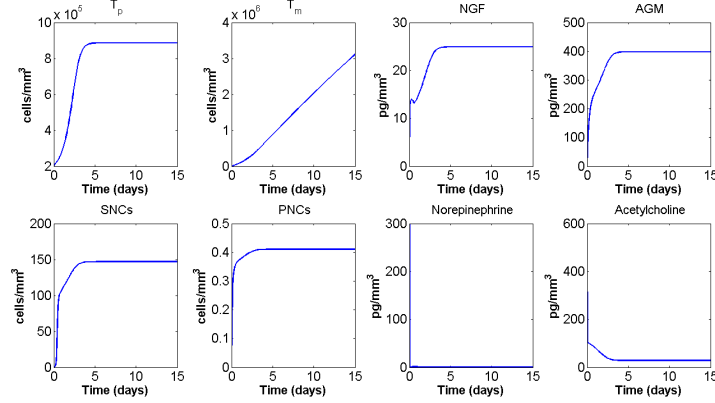


FIGURE 2. Time-course of the model variables over a period of 15 days for $T_0^{20\%}$.

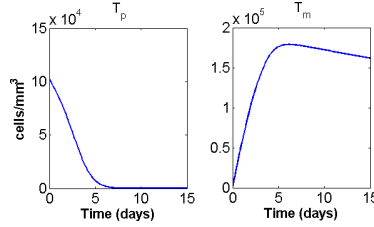


FIGURE 3. Primary and migrating tumor cells density time-course for initial condition $T_0^{10\%}$.

this model tumor cell survival and growth are affected only by nerves, while in reality blood vessels also contribute to tumor maintenance by providing oxygen and nutrients; this may (partially) account for the high threshold.

4.1. PSA. To test the robustness of the model, we performed a parameter sensitivity analysis (PSA) by observing the effect that a 10% increase/reduction of each parameter value has on tumor cell densities at day 15. The model appears to be very solid in the sense that final tumor cell densities are not greatly affected by perturbations in the parameter values. The only parameters that generate a change in migrating tumor cells of 2% or more are reported in Figure 4. Of these, only k_T has a similar effect on primary tumor cells.

4.2. Stress and tumor progression. Many cancer patients exhibit stress and depression, which are known to have an effect on the immune system and consequently tumor growth [59,87]. Additionally, they may have a direct effect as stress is associated with increased release of norepinephrine by the hypothalamus and sympathetic nerves [36, 45, 64]. Here we simulate a stress condition by increasing the norepinephrine release rate s_n by sympathetic nerves. Figure 5A shows the time course

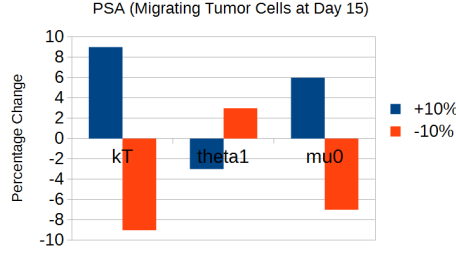


FIGURE 4. Parameter sensitivity analysis. The graph shows the effects on migrating tumor cells at day 15 after an increase (blue) or decrease (orange) of 10% in the parameters. Here only the parameters which induced a percentage change of 2% or more are shown.

of primary and migrating tumor cells when s_n is multiplied by 10 for initial condition $T_0^{20\%}$. The plots show that when s_n is increased, the primary tumor cell density settles quickly to a higher equilibrium, while tumor cell migration is enhanced. This is in accordance with the experimental observation that stress is related to higher cancer metastasis and perhaps higher mortality [13, 58]. Again, our results agree qualitatively (but not quantitatively) with the experimental evidence.

Another interesting prediction of our model is that for some initial conditions, such as $T_0^{10\%}$, stress makes a crucial difference in tumor development. Here, if s_n is taken to be its baseline value, recall the primary tumor tends to zero (Figure 3); in stress conditions (simulated by multiplying s_n by 10) the same initial condition leads to primary tumor growth and a constant increase of migrating tumor cells (Figure 5B). This observation suggests that a stressful environment can affect tumor development and therapeutic efficacy, in accordance with many findings in the biological literature [25, 87]. More experimental data are needed to precisely quantify this effect, however this already supports the potential for treatments targeting the sympathetic nervous system, as discussed in [15].

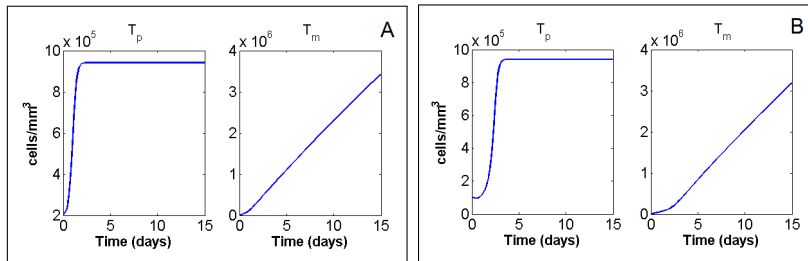


FIGURE 5. Primary and migrating tumor cells in stress conditions (simulated by multiplying s_n by 10) for initial conditions (A) $T_0^{20\%}$ and (B) $T_0^{10\%}$ respectively.

4.3. Blocking tumor acetylcholine receptors. Regarding parasympathetic neural activity, it is reported in [54] that impairing the cholinergic (acetylcholine) receptors on tumor cells does not significantly affect tumor growth in the orthotopic site, but markedly reduces tumor cell spreading and metastasis. To simulate this phenomenon, we set $\mu_2 = 0$; that is, we consider tumor cells to be non-responsive to acetylcholine. The output is shown in Figure 6, where we see a slower increase in the migrating tumor cells. The model corroborates the findings of [54] that cholinergic receptors on tumor cells are potential clinical targets in view of limiting cancer metastasis.

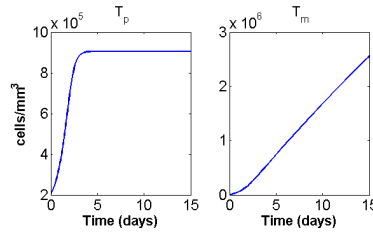


FIGURE 6. Primary and migrating tumor cells when acetylcholine receptors on tumor cells are blocked ($p_0 = 0.4$); this scenario is simulated by setting $\mu_2 = 0$.

5. DISCUSSION

This work is the first mathematical confirmation of the major role played by the autonomic nervous system in promoting tumor development and progression of prostate cancer and highlights neurogenesis as a target for cancer drug development. In the present paper we develop a simple mathematical model for tumor neurogenesis and cancer progression based on recent experimental evidence; it results that, regardless of the presence of angiogenesis and lymphangiogenesis, tumor-induced neurogenesis represents a symbiotic factor for prostate tumor. This work further expands our understanding of the process by which stress can regulate cancer aetiopathogenesis: previous research predominantly emphasized the role of the immune system in mediating stress effects on tumor growth and metastasis, while our model predicts that stress can directly affect primary tumor growth through the release of neurotransmitters. In addition, the effect of parasympathetic nerves is also captured by the model through the acetylcholine-induced tumor migration.

This model, though quite simple, gives good insights into tumor neurogenesis and offers many possibilities for expansion and improvement. First of all, the introduction of a spatial variable and thus

the use of PDEs would allow a more precise description of the processes occurring during tumor neoneurogenesis. In particular, a spatial approach may be able to explain why sympathetic nerves tend to accumulate in normal tissues and only penetrate tumor edges, while parasympathetic nerves infiltrate tumor tissues [54]. Also, a more accurate description of the spatial component could allow for a distinction between axon elongation and nerve cell proliferation [2].

The model could be further improved by considering different variables for different kinds of AGMs, which are known to have diverse effects on tumor cells [11]. In fact, circulating tumor cells are probably attracted to a specific organ by chemokines and AGMs; the fate of a new tumor cell cluster will depend on the sensitivity of the tumor cells to the specific factors and AGMs produced in the new environment.

One could also take into account the blood and lymphatic vasculatures. Guidance cues for axons also have a function in (lymph)angiogenesis [9, 24, 92]. Both angio-, lymphangio- and neoneuro-genesis promote metastasis formation, although in different ways; for instance, blood and lymphatic vessels offer pathways for tumor cells to disseminate, similar to perineural invasion [28].

Another factor that could be included in the model is the immune system, which functions as a bridge between the tumor and nervous system and is the main cause of the *indirect* connections between the two (in addition, NGF also seems to be involved in immune response and inflammation [23, 91]).

ACKNOWLEDGMENT

The authors would like to thank Dr. Lasse Jensen, Dr. Kevin Painter and Prof. Michael Pepper for the useful technical discussions and suggestions.

APPENDIX A. PARAMETER ESTIMATION

A.1. Standard sizes and weights.

Domain and normal prostate sizes. We take normal prostate size to be approximately $30\text{mL} = 3 \times 10^4\text{mm}^3 = V_{\text{prost}}$ [62]. Assuming a spherical shape, this implies a radius of about 20 mm.

For our model, we consider the prostate and its surroundings. Therefore we consider a slightly bigger sphere, with the same centre; say (for instance) of radius 25 mm. This leads to a domain volume $V_{\text{dom}} = 65.45 \times 10^3\text{mm}^3$.

Tumor cell size. In [66] the circulating tumor cells and the cultured tumor cells in prostate cancer patients are measured; the first ones are found to have an average diameter of $7.97\text{ }\mu\text{m}$, while the latter of $13.38\text{ }\mu\text{m}$. We then take a tumor cell diameter of $10\text{ }\mu\text{m} = 10^{-2}\text{mm}$ and thus of approximate volume $V_{\text{tum cell}} = 5 \times 10^{-7}\text{mm}^3$.

Neurite diameter and nerve cell size. Take neurite diameter to be about $1\ \mu\text{m}$ [32, Table 2.1]. In [34] human Purkinje cell⁴ diameter is reported to be $27\ \mu\text{m}$. We then estimate the nerve cell volume to be approximately $10^{-5}\ \text{mm}^3$.

NGF molecular weight. In [70] and PhosphoSitePlus NGF molecular weight is stated to be $26 \times 10^3\ \text{Da}$. However, NGF molecular weight is estimated to be between 10^4 and $10^5\ \text{Da}$ in [3, 60]. We will then assume the intermediate value $10^4\ \text{Da} \approx 1.660 \times 10^{-8}\ \text{pg}$.

AGM molecular weight. Molecular weight of Semaphorin 4D is 96,150 Da (see product at www.abcam.com). Netrin-1 molecular weight is 75 kDa = $1.245 \times 10^{-7}\ \text{pg}$ [55].

Noradrenaline molecular weight. NE molecular weight = 169.17784 g/mol (from PubChem).

A.2. Equilibrium values.

Initial primary tumor cell densities $T_0^{20\%}$, $T_0^{10\%}$. If we take an initial density of primary tumor cells corresponding to a certain percentage p_0 of the prostate volume, we have that

$$T_p(0) = \frac{p_0 \times V_{\text{prost}}}{V_{\text{tum cell}}} \times \frac{1}{V_{\text{dom}}} = p_0 \times 10^6.$$

Taking $p_0 = 0.20$ and $p_0 = 0.10$ we have the initial conditions $T_0^{20\%}$ and $T_0^{10\%}$, respectively.

Sympathetic and parasympathetic nerve density. In [54, Figure 7 A,D] we find a quantification of sympathetic and parasympathetic (respectively) neural areas in normal human prostate tissues. From the graph, one can take a positive nerve area per field of about $1000\ \mu\text{m}^2$ for sympathetic and $100\ \mu\text{m}^2$ for parasympathetic fibers, field surface = $0.15\ \text{mm}^2$. It follows that the percentage of the area occupied by nerve fibers is approximately 0.7% and 0.07 % for sympathetic and parasympathetic nerves respectively. Note that here a section is $5\ \mu\text{m}$ thick. However, the staining here identify any kind of nerve fibers, and it is well known that axon size is extremely variable depending on the type (for instance, in [34] it is recorded a nerve diameter of $27\ \mu\text{m}$, while [76] reports a nerve fiber layer thickness in the eye of about $100\ \mu\text{m}$). We will assume that the nerve fibers occupy the whole thickness of the sections; thus we conclude that sympathetic nerves account for 0.7% of the normal prostate tissue volume and parasympathetic ones for 0.07%.

To convert these values in an actual cells/ mm^3 value, we recall that in A.1 we found a domain volume of $65,450\ \text{mm}^3$. Taking the above found percentages of volume occupied by neural fibers, we have $458.1500\ \text{mm}^3$ occupied by sympathetic nerves and $45.8150\ \text{mm}^3$ by parasympathetic

⁴**Purkinje cells:** a class of nerve cells

ones. Approximating a nerve cell a sphere of $27 \mu\text{m} = 27 \times 10^{-3} \text{ mm}$ diameter [34], we have that 458.1500 mm^3 correspond to 16,969 cells and 45.8150 mm^3 to 1,697 cells. Therefore, the initial sympathetic nerve density will be $S^{eq} = 16,969/65,450 \approx 0.26 \text{ cells/mm}^3$ and the initial parasympathetic nerve density $P^{eq} = 1,697/65,450 \approx 0.03 \text{ cells/mm}^3$.

Noradrenaline level. In [82] the endogenous noradrenaline level in different rat gastrointestinal tissues was measured. Taking the approximate average value $0.3 \mu\text{g/g}$ and density of the tissue equal to water's (i.e. $1\text{g}=1\text{mL}$), we have that this corresponds to $N_n^{eq} = 0.3 \times 10^3 \text{ pg/mm}^3$.

Acetylcholine level. In [61] small intestine and kidney acetylcholine levels are assayed in choline-deficient and normal weanling Fischer germfree⁵ and open-animal-room rats; it results that acetylcholine levels of the choline-supplemented germfree and open-animal-room rats were similar in both sites. In particular, in [61, Table 1] we find that in germfree rats acetylcholine levels in small intestine and kidneys are $0.82 \mu\text{g/g}$ and $0.24 \mu\text{g/g}$, respectively. Taking the average of these values and considering a density equal to water's one (1g/mL) we get the "basal" acetylcholine level $N_a^{eq} = 530 \text{ pg/mm}^3$.

A.3. T_p -equation.

Tumor constant growth rate r_T . In [75] is reported that prostate cancer has a very large doubling time. In particular: "Seventy-nine percent of all patients had a doubling time of more than 24 months. Twenty of 28 cancers thought to be clinically organ confined doubled at rates exceeding 48 months". We could then take $r_T = \ln 2/48\text{months} \approx 4.81 \times 10^{-4} \text{ day}^{-1}$.

Tumor constant death/apoptotic rate d_T . In [18] the apoptotic index (AI) of prostatic adenocarcinoma was calculated as

$$\text{AI (\%)} = 100 \times \text{apoptotic cells/total cells}.$$

The mean AI in 3,000 tumor nuclei was 1.27. We will therefore take $d_T = 1.27 \times 10^{-2}$.

To compare these *growth and death rates* with others, we see that in [79] it is stated that "The growth rate constants varied over a nearly 1,500-fold range, while the regression rate constants varied over a 50-fold range (Figure 3A). Furthermore, the regression rate constants were consistently larger than the growth rate constants, with median values of $10^{-1.7} \text{ day}^{-1}$ versus $10^{-2.5} \text{ day}^{-1}$, respectively." These observations correspond to $r_T \approx 10^{-2.5} \text{ day}^{-1}$ and $d_T \approx 10^{-1.7} \text{ day}^{-1}$. Now, while d_T is approximately the same computed above, r_T here is bigger; this

⁵NOTE: The term "germfree" here refers to rats free from viable bacteria, parasites, or fungi.

difference is explained by the fact that prostate tumor is well-known for being particularly slow in growth.

NGF-enhanced tumor growth τ_1, τ_2 . In [93, Figure 4A] the authors report the dose-dependent effects of NGF on pancreatic cancer cell growth *in vitro* after 48 hours. Here data are expressed as a percentage of increase or decrease of untreated controls. In particular, the data in Table 3 are recorded.

NGF (ng/mL)	% increase of untreated controls
6.3	approx. 130
25	approx. 180
100	approx. 210

TABLE 3. (Recall: 1 ng/mL = 1 pg/mm³.) Time = 48 hours = 2 days.

We then consider the NGF-dependent growth part in the T_p -equation

$$\frac{dT_p}{dt} = \left(r_T + \frac{G}{\tau_1 + \tau_2 G} - d_T \right) \cdot T_p$$

that, assuming G constant, has solution

$$T(t) = T_0 \exp \left[\left(r_T + \frac{G}{\tau_1 + \tau_2 G} - d_T \right) \cdot t \right] \quad (9)$$

that for $G = 0$ reduces to

$$T(t) = T_0 \exp [(r_T - d_T) \cdot t] , \quad (10)$$

which will correspond to the control case.

Now, from the data in Table 3 we see that if, for example, $G = 6.3$, then

$$\frac{T_{G=6.3}(t=2)}{T_{G=0}(t=2)} = \exp \left[\frac{G}{\tau_1 + \tau_2 G} \cdot t \right] = 1.3 .$$

Similarly

$$\frac{T_{G=25}(t=2)}{T_{G=0}(t=2)} = 1.8 \quad \text{and} \quad \frac{T_{G=100}(t=2)}{T_{G=0}(t=2)} = 2.1 .$$

We thus have a system of three equations in two unknowns τ_1, τ_2 :

$$\begin{cases} \ln(1.3) [\tau_1 + 6.3 \cdot \tau_2] = 2 \cdot 6.3 \\ \ln(1.8) [\tau_1 + 25 \cdot \tau_2] = 2 \cdot 25 \\ \ln(2.1) [\tau_1 + 100 \cdot \tau_2] = 2 \cdot 100 \end{cases} \quad (11)$$

From the second equation in (11) we get $\tau_1 = 85.06 - 25 \cdot \tau_2$. Substituting this expression in the first equation gives $\tau_2 = 1.98$ and consequently $\tau_1 = 35.56$; doing the same with the last (third) equation in (11) gives $\tau_2 = 2.46$ and $\tau_1 = 23.56$. Taking the averages we get $\tau_1 = 30.74$ and $\tau_2 = 2.27$. However, these values give rise to an unrealistically big tumor cell growth; therefore, in our simulations we will

take these two values to be multiplied by 10, thus having $\tau_1 = 307.4$ and $\tau_2 = 22.7$. This difference is justified by the fact that the dataset we used for our fit refers to pancreatic tumor cells, while in the paper we focus predominantly on prostate cancer.

Maximum tumor cell density k_T . The maximum tumor cell density is given by $1\text{mm}^3/V_{\text{tum.cell}} = 2 \times 10^6$; in fact, k_T corresponds to the maximum number of tumor cells that can fit in every mm^3 . Now, because of the presence of the stroma and other cells not implicitly included in the model, we will take half of this value $k_T = 1 \times 10^6$ cells/ mm^3 .

Shape of $\vartheta(N_n)$ and values of θ_1, θ_2 . We want the function $\vartheta = \vartheta(N_n)$ to be such that $\vartheta(0) \neq 0$ (to reflect the presence of an Allee threshold in the presence of a strong Allee effect) and that ϑ is a decreasing function of N_n (in fact, our hypothesis is that norepinephrine lowers the Allee threshold, making the tumor more likely to proliferate). We thus consider $\vartheta(N_n) = \theta_1/(1 + \theta_2 N_n)$, where θ_1 and θ_2 are two parameters to be determined.

For θ_2 , we consider [12, Figure 1], where the time course of prostate tumor weight is shown in control mice and in mice treated with doxazosin, an $\alpha 1$ -adrenergic-antagonist (α -blocker). In the plot, we observe that in the doxazosin-treated mice the tumor weight dropped down from about 5 g to zero, while in control mice a tumor of weight around 2 g kept growing. Assuming that the doxazosin treatment blocked all the adrenergic receptors on tumor cells (thus corresponding to the case $N_n = 0$), and that in the control experiment the norepinephrine was at its equilibrium value N_n^{eq} , we deduce that

- when $N_n = 0$ (i.e. norepinephrine does not make any effect on tumor growth), 5 g is *below* the Allee threshold;
- when $N = N_n^{eq}$, 2 g is *above* the Allee threshold.

Now, since it is difficult to translate these tumor weights in tumor cell densities (mouse prostate size and tumor cell size are probably different from human ones), we can only use the “relative” information contained above, that is

$$\left. \begin{array}{l} \theta_1 > 5 \text{ g} \\ \frac{\theta_1}{1 + \theta_2 N_n^{eq}} < 2 \text{ g} \end{array} \right\} \Rightarrow 1 + \theta_2 N_n^{eq} > \frac{5}{2} \Rightarrow \theta_2 > 5 \times 10^{-3} \frac{\text{mm}^3}{\text{pg}}.$$

We can take for instance $\theta_2 = 1 \text{ mm}^3/\text{pg}$.

As pointed out in [43], no experiment has been done to measure the “basal” Allee threshold θ_1 for any kind of tumor. We will just assume that θ_1 is approximately the 1% of the carrying capacity k_T , i.e. $\theta_1 = 1 \times 10^4$.

AGM-induced tumor cell apoptosis δ . In [10, Table 1] we find a quantification of the effect of semaphorin 3B on two different kinds of cancer cells; these data are summarised in Table 4.

Treatment	H1299 lung cancer cells	MDA-MB-231 breast cancer cells
Control-CM	11×10^4	16×10^4
SEMA3B-CM	6×10^4	5×10^4

TABLE 4. Time = 5 days; $C_0 = 10^4$ cells/well (six-well plates)

We will then consider the following two equations for control tumor cells $T_{control}$ and for semaphorin-treated ones T_{SEMA} :

$$T_{control}(t) = T_0 \exp[(r_T - d_T)t] \quad \text{and} \quad T_{SEMA}(t) = T_0 \exp[(r_T - d_T - \delta A)t],$$

where A represents the concentration of axon guidance molecule (here, semaphorin). To estimate A we consider the statement “Semiquantitative assay showed an average of 15–40 ng/mL SEMA3B in the C-Mafer transfection” in the *Materials and Methods* section and the fact that the medium was diluted 1:2; in this way we approximate $A \approx 13.75 \text{ pg/mm}^3$ (note that $1 \text{ ng/mL} = 1 \text{ pg/mm}^3$). Equipped with all these values (recall: $t = 5$), we can use the data in Table 4 as follows:

$$\text{H1299 cells: } \frac{T_{SEMA}}{T_{control}} = \exp(-\delta A t) = \frac{6}{11}, \quad \text{MDA-MB-231 cells: } \frac{T_{SEMA}}{T_{control}} = \frac{5}{16}$$

and then calculate the corresponding δ values 0.0088 and 0.0169 respectively. Taking the average, we get $\delta \approx 1.29 \times 10^{-2}$.

Spontaneous tumor cell migration μ_0 . In [69] about 1,400 colonies of (rat) prostate tumor cells are observed after 8 days (see Figure 4 in the same reference). Without knowing how big each colony is, we will assume that 1 colony corresponds to 1 cell. Therefore, taking an exponential decay $T_p(t) = T_p(0) \exp(-\mu_0 t)$ for the tumor cells and knowing that the initial cell density was $T_p(0) = 2 \times 4 \times 10^3 \text{ cells/mL}$ (stated also in [69]), we can calculate $\mu_0 = 0.22 \text{ day}^{-1}$.

AGM-induced migration μ_1 . In [38, Figure 3] the following % cell invasion are reported for semaphorin-treated PC-3 cells⁶:

$$\text{sema3A: } \sim 65\% \text{ of control} \quad , \quad \text{sema3C: } \sim 135\% \text{ of control}$$

after 20 hours incubation ($T_0 = 10^5$). The authors’ comment is: “Overexpression of sema3A in PC-3 decreased the invasive characteristics of PC-3 cells by 33% compared to the untransfected cells. Sema3C, on the other hand, increased invasion by 33% compared to untransfected cells”. To estimate the amount of semaphorin used in the experiment, we read: “The bacterial clones transfected with sema3A or sema3C were grown on agar plates and selected with $35 \text{ } \mu\text{g/mL}$

⁶**PC-3 cells:** androgen-independent prostate cell line.

of kanamycin". Therefore, in our equation for tumor cell migration $T_m(t) = T_0 \exp[(\mu_0 + \mu_1 A)t]$ we will take $A = 35 \mu\text{g/mL} = 35 \times 10^3 \text{ pg/mm}^3$. Finally, considering the 20-hours sema3C treatment, we have that

$$\frac{T_0 \exp[(\mu_0 + \mu_1 A)t]}{T_0 \exp(\mu_0 t)} = 1.33 \quad \Rightarrow \quad \mu_1 A t = \ln(1.33) \quad \Rightarrow \quad \mu_1 = 9.8 \times 10^{-6} \frac{\text{mm}^3}{\text{pg} \cdot \text{day}}.$$

Acetylcholine-induced migration μ_2 . [54, Figure 3A] reports an *ex vivo* quantification of tumor cell invasion of pelvic lymph nodes (which drain the prostate gland). Here data are reported both for control (saline-treated) and carbachol-treated mice, and in the second case the invading tumor cells are about the double than in the control. Notice that since carbachol is a non-selective cholinergic (muscarinic) receptor agonist, we can consider it as a substitute of acetylcholine. Then, denoting with c the carbachol amount, we can estimate from the equation $T_m(t) = T_0 \exp[(\mu_0 + \mu_2 N_a)t]$ and [54, Figure 3A] that $\mu_2 c t = \ln(2)$ (since $T_0 \exp[(\mu_0 + \mu_2 c)t] \approx T_0 \exp(\mu_0 t)$). To estimate the value of c , we read in [54]: "For experiments on the PNS, 15 days after tumor cell injection, animals received carbachol at 250 (day 0), 300 (day 1), 350 (day 2), 500 $\mu\text{g/kg}$ per day (day 3) [every 12 hours, 8 divided doses]". First notice that the average of these amounts is 350 $\mu\text{g/kg}$ over 5 weeks, which corresponds to 10 $\mu\text{g/kg/day}$. To convert the kilos in a volume, we take water density (1 g/mL); therefore we find the approximation $c = 10 \text{ pg/mm}^3/\text{day}$ and thus $\mu_2 = 2 \times 10^{-3} \text{ mm}^3 \text{pg}^{-1} \text{day}^{-1}$ ($t = 35$ days).

A.4. G -equation.

NGF decay rate d_G . In [81] is stated that "Nerve growth factor (NGF) mRNA is rapidly degraded in many non-neuronal cell types with a half-life of between 30 and 60 min". Hence, taking a half-life of 45 minutes, the resulting decay rate is $d_G = 0.0154 \text{ min}^{-1} = 22.18 \text{ day}^{-1}$.

NGF production by tumor cells s_G . In [20, Figure 1c] it is reported that after 24 hours, cultures of different lines of breast cancer cells expressed approximately 0.3 ng/(mg protein) of NGF. Considering a total protein amount of 300 pg per cell (as in HeLa cells⁷), we have that 1 mg = 10^9 pg protein corresponds to approximately 3×10^6 cells. Now, we have to consider that in 24 hours the NGF also decayed; in fact the differential equation for G in this case is

$$\frac{dG}{dt} = s_G T - d_G G \quad \Rightarrow \quad G(t) = \left(G(0) - \frac{s_G}{d_G} T \right) \exp(-d_G t) + \frac{s_G}{d_G} T$$

⁷**HeLa cells:** an immortalised cell type used in biological research, derived from cervical cancer cells taken from Henrietta Lacks, who eventually died of her cancer in 1951.

where T denotes the number of tumor cells (and $G(0) = 0$ in our case). Thus, [20] tells us that $G(t = 1\text{day}) = 0.3 \times 10^3 \text{pg}$, $T = 3 \times 10^6 \text{cells}$. Substituting these numbers in the equation (and taking the value of d_G estimated above), we determine $s_G = 2.22 \times 10^{-3} \text{pg} \cdot \text{cells}^{-1} \cdot \text{day}^{-1}$.

NGF internalization rate by tumor cells γ_1 . In [71, Table 1] it is reported the internalization of ^{125}I -NGF after 1 hour or 24 hours incubation of different cell lines with 10 ng/mL. For SKBr5 breast carcinoma cells, we find that 33,560 molecules/cell were internalised after 24 hours incubation. Considering a NGF molecular weight of $1.660 \times 10^{-8} \text{pg}$ and knowing that the cells were seeded at density $2 \times 10^7 \text{cells}/10 \text{mL} = 2 \times 10^3 \text{cells}/\text{mm}^3$, we can write down the equality

$$\gamma_1 \times \left(2 \times 10^3 \frac{\text{cells}}{\text{mm}^3}\right) \times \left(10 \frac{\text{pg}}{\text{mm}^3}\right) = 33.56 \times 10^3 \times 1.660 \times 10^{-8} \frac{\text{pg}}{\text{mm}^3} \times 2 \times 10^3 \text{cells} \frac{1}{\text{day}},$$

which leads to $\gamma_1 = 5.57 \times 10^{-5} \text{mm}^3 \text{cells}^{-1} \text{day}^{-1}$.

NGF internalization rate by nerve cells γ_2 . We can estimate the rate of NGF internalization by cultured neurons using the data in [14, Figure 1]. The plot reports the pg of ^{125}I -NGF binding to rat sympathetic neurons versus different amounts of free NGF. It is also stated that the neurons were incubated for 140 minutes with the NGF at a density of approximately 1,000 neurons/dish in 35-mm culture dishes.

Therefore, if we have a density of free NGF equal to G_0 , the corresponding value on the y -axis of [14, Figure 1] corresponds to $G(t = 140\text{min}) = G_0 \exp(-\gamma_2 St)$. Then, converting these data into our units, we can use the MatLab functions `nlinfit` and `nlparci` to get an estimate for γ_2 and its 95% confidence interval respectively. The plot of the fit is reported in Figure 7 and the output is:

```
>> claude.ngf = [5 20 40 60]
>> claude.binding = [4.98 19.95 39.90 59.865]
>> NGFinternFIT(claude)
Estimated gamma2 value = 0.048342
ci for gamma2 =      0.0422      0.0545
```

A.5. A-equation. A large class of secreted or membrane bound axon guidance molecules are semaphorins and more specifically the so called class-3 semaphorins, that include seven family members. Class 3 semaphorins are the only secreted vertebrate semaphorins. In a recent work, the authors of [7] highlighted that Semaphorin 3E is not only overexpressed in prostate cancer but also affects adhesion and motility of prostate cancer cells. They also demonstrated that all the prostate cancer cell lines that have been tested produce both the unprocessed (87kDa) and processed (61kDa) form of Sema3E. However the effect of tumor and

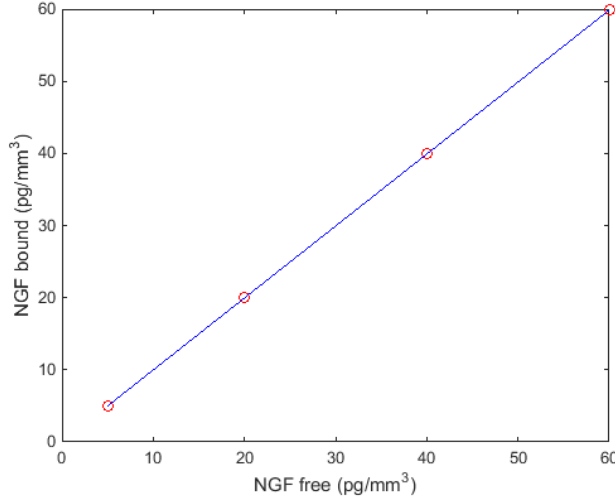


FIGURE 7. Plotting the data from [14] (red circles) together with the function $G(t) = G_0 \exp(-\gamma_2 St)$ (blue line) fitted to the data with the MatLab function `nlinfit`.

stromal secreted semaphorins on tumor functionalities such as migration, apoptosis, growth and invasion is likely to depend on which co-receptors are expressed. Namely, sema3E act as a chemoattractant for neurons expressing NRP1 receptors, that have been found to have a high expression on prostate tumors.

AGM tumor secretion rate s_A . In [42] the concentration of secreted sema3s in conditioned medium is estimated for specific tumor cell lines. As it can be deduced by [42, Figure 2] the relative concentrations of class-3 semaphorins secreted into the medium of tumor cell lines were 1000 and 500 sema3-expression per cell. Tumor cells were incubated for 48 hours = 2 days. Take an average of the aforementioned values, we deduce that the expression of sema3 pre-cell per-day is 350. Taking the molecular weight of unprocessed sema3 to be 87kDa (as described at the beginning of this section A.5), we estimate that the secretion rate is: $s_A = 350 \times 87000 \times 1.66 \times 10^{-12} \text{pg cell}^{-1} \text{day}^{-1}$, thus $s_A \approx 5.055 \times 10^{-5} \text{pg cell}^{-1} \text{day}^{-1}$. However, in [42] it is highlighted that the aforementioned expressed semaphorins did not affect the proliferation rate or the survival of the different semaphorin tumor producing cells. In this regard, we expect that during tumor driven neo-neurogenesis the expressed tumor secreted sema3E are 100 or 1000 higher than the estimated value, in other words we take $s_A = 5.06 \times 10^{-3} \text{pg cell}^{-1} \text{day}^{-1}$.

AGM decay rate d_A . In [77, Supplementary Tables 1 and 2] we find the mRNA half-life of different kinds of semaphorins. We take an average decay rate of $0.1 \text{ h}^{-1} = 2.4 \text{ day}^{-1}$.

In [55] we read: “Currently, little is known about the half-life of netrin-1 protein in any context”.

AGM internalization by nerve cells γ_4 . In [41, Figure 4] it is studied the binding of netrin(VI●V)-Fc to DCC-expressing cells (spinal commissural axons). Here the c.p.m. are reported for different concentrations of netrin. Assuming the every binding corresponds to 1 molecule, and taking the netrin molecular weight 1.245×10^{-7} pg, we can calculate the decrease of *free netrin*, that in our system is represented by the variable A and in this case is modelled by the equation $A(t) = A_0 \exp(-\gamma_4 St)$. Then, having $S = 2.5 \times 10^5$ cells/24-well = 71.43 cells/mm³ (24-well \rightarrow 3.5 mL) and $t = 1$ minute = 6.9444×10^{-4} days, we can fit this as a function of A_0 , as in [41, Figure 4]. The MatLab functions `nlinfit` and `nlparci` give the following γ_4 estimate and 95% confidence interval:

```
>> keino.netrin = [0 1 2 5 10].*10^3
>> keino.binding = [0.5 1.5 3.5 4.5 4.5].*10^4
>> AGMinternFIT(keino)
Estimated gamma4 value = 1.4673e-005
ci for gamma4 = 1.0e-004 * [ 0.0462 0.2472 ]
```

The plot of this fitting is reported in Figure 8.

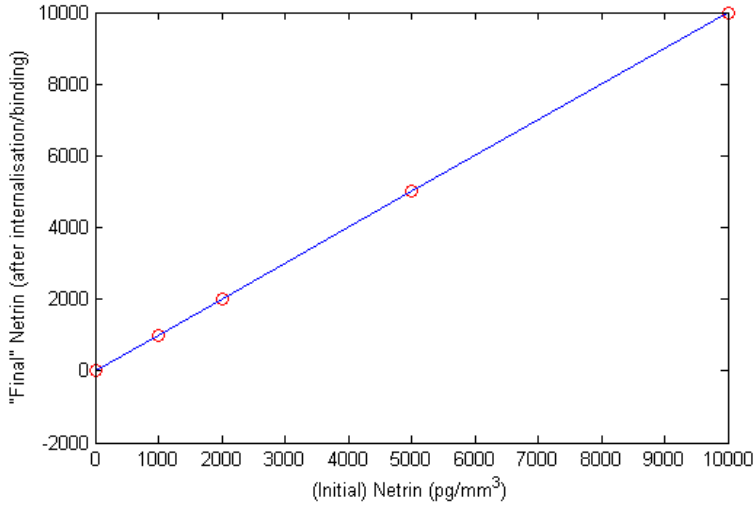


FIGURE 8. Plotting the data from [41] (red circles) together with the function $A(A_0) = A_0 \exp(-\gamma_4 St)$ (blue line) fitted to the data with the MatLab function `nlinfit`.

A.6. S -equation.

Basal SNC growth rate r_S . In [20, Table 1] we find that 4.4% control sympathetic neurons cultured for 48 hours showed a neurite length of 29 μm . The initial cell density was 2×10^3 cells/well that, assuming a well volume of 100 μL , correspond to $S_0 = 2 \times 10^{-2}$ cells/ mm^3 ; moreover, taking a neurite diameter of 1 μm , we have that 29 μm neurite correspond to approximately 2.9 cells (recalling that we consider a nerve cell volume of about 10^{-5}mm^3).

From [20]: “Cell culture plates (96-well) were prepared by incubating each well with 100 μL of 0.1mg/mL poly-L-lysine in sterile distilled water [...] Approximately 2×10^3 cells, prepared from embryonic day-12 chick paravertebral sympathetic ganglia, were added to each well in 100 μL of a 1:1 mixture of [...] medium”.

Hence, we conclude that after 2 days of experiment there were

$$S(t=2) = S_0 + 0.044 \times S_0 \times 2.9 \text{ cells} \Rightarrow S(t=2) = 2.2552 \times 10^{-2} \text{ cells}/\text{mm}^3 = S_0 \exp(2 \cdot r_S)$$

from which we can calculate $r_S = 0.06 \text{ day}^{-1}$.

SNC carrying capacity k_S . In absence of tumor, we know that the SNC equilibrium value is $S^{eq} = 0.26 \text{ cells}/\text{mm}^3$ (see section A.2). We then take $k_S = S^{eq}$.

NGF-enhanced SNC growth σ_1, σ_2 . In [74, Table 1] the effects of NGF treatment on superior cervical ganglion cell dendritic morphology are reported; they are summarised here in Table 5.

Treatment	Animal size	Total dendritic length (μm)
Control	23.5 g	721
NGF	23.5 g	929

TABLE 5. Mouse 2.5S NGF was administered daily to mice by subcutaneous injection in a dosage of 5 mg/kg. The animals were treated for 2 weeks.

Now, if we take a dendritic diameter of 1 μm and a nerve cell volume of 10^{-5} mm^3 , we have that 1 μm dendrite corresponds to about 10^{-4} cells. Therefore, we can “convert” the previous dendritic lengths in cells (at least roughly). For the NGF treatment, we know that it was 5 mg/kg/day for 2 weeks. If a mouse was 23.5 g, we have that each animal received $117.50 \times 10^6 \text{ pg/day}$. Being NGF injected subcutaneously, we assume that only 1% of the dosage actually contributed to the experiment (the rest being dispersed by body fluids). Additionally, we estimate a total mouse volume of $28.57 \times 10^3 \text{ mm}^3$ (knowing that mice blood volume is about 2 mL and it constitutes 7-8% of their total volume [85]) and thus we have a daily NGF supply of $41.13 \text{ pg}/\text{mm}^3/\text{day}$. Now, to calculate the effective NGF present, we have to take into account its decay. We know that NGF decay rate is $d_G = 22.18 \text{ day}^{-1}$

(see A.4); if we define the constant supply $s = 41.13 \text{ pg (mm}^3\text{)}^{-1}\text{day}^{-1}$, we have that the evolution equation for G in this setting is

$$\frac{dG}{dt} = s - d_G G \implies G(t) = G_0 e^{d_G t} - \frac{s}{d_G} e^{-d_G t} + \frac{s}{d_G}.$$

Then, taking $G_0 = 0$, we have that at $t = 1$ day the amount of NGF is approximately 1.85 pg/mm^3 . For the two-week experiment, we will then assume G to be $1.85 \times 14 = 25.96 \text{ pg/mm}^3$. Then, back to the S -equation: we recall that the bit in which we are now interested is

$$\frac{dS}{dt} = \left(r_S + \frac{G}{\sigma_1 + \sigma_2 G} \right) S \xrightarrow{G \text{ const}} S(t) = S_0 \exp \left[\left(r_S + \frac{G}{\sigma_1 + \sigma_2 G} \right) t \right]$$

we have that at 2 weeks = 14 days

$$\frac{S_{NGF}}{S_{control}} = \exp \left(\frac{G}{\sigma_1 + \sigma_2 G} \times 14 \right) = \frac{929}{721} = 1.29.$$

From this equation (recall: $G = 25.96$) we derive $\sigma_1 = 25.96 \times (54.9791 - \sigma_2)$. Consequently, we have that it must be $\sigma_2 < 54.9791$ in order to have $\sigma_1 > 0$.

We can derive a second equation for σ_1 and σ_2 from the experimental results reported in [17]. In fact, [17, Table 1] lists the maximal effects on neurite lengths of various additions to the culture medium. In particular, the mean total neurite length per neuron after different treatments divided by the corresponding value of the untreated control is reported. For sympathetic neurons exposed for 2 hours to 1 ng/mL NGF, the relative length is 2.47; this observation allows us to write the following equality:

$$\exp \left(\frac{G}{\sigma_1 + \sigma_2 G} \times 0.0833 \right) = 2.47 \implies \sigma_2 = 57.1782,$$

the latter obtained after substituting the expression for σ_1 found previously (note that 2 hours = 0.0833 days). Notice that although σ_2 is bigger than 54.9791, the difference is small (less than one order of magnitude). This is probably due to the fact that the two references used to estimate σ_1, σ_2 deal with completely different experimental settings (for example, the experiment done in [74] is *in vivo* while [17] is *in vitro*). Therefore it seems justified to take for instance $\sigma_2 = 50$ days and consequently $\sigma_1 \approx 129 \text{ pg day (mm}^3\text{)}^{-1}$.

AGM-enhanced SNC growth σ_3, σ_4 . In [44, Figure 1A(ii) and 2A] the synapse density after 0.5, 1, 2 and 4 hours of Sema4D treatment is reported as % of control. In particular, it is reported that after 0.5 hours = 0.0208 days = t_1 of 1nM-Sema4D-treatment GABAergic synapse formation in rodent hippocampus was about 130% of control, and after 1 hour = 0.0417 days = t_2 it was approximately 150% of control. Now,

recalling the “growth bit” of the S -equation

$$\frac{dS}{dt} = \left(r_S + \frac{A}{\sigma_3 + \sigma_4 A} \right) S \xrightarrow{A \text{ const}} S(t) = S_0 \exp \left[\left(r_S + \frac{A}{\sigma_3 + \sigma_4 A} \right) t \right],$$

we have from the previous datapoints that

$$\exp \left(\frac{At_1}{\sigma_3 + \sigma_4 A} \right) = 1.3 \quad \text{and} \quad \exp \left(\frac{At_2}{\sigma_3 + \sigma_4 A} \right) = 1.5$$

(since the control corresponds to the $S(t)$ where $A = 0$). Note that taking molecular weight of 96,150 Da for A , we have that $A = 1 \text{ nM} = 96.117 \text{ pg/mm}^3$. Finally, considering the average of the two expressions above we can estimate

$$\sigma_3 + \sigma_4 A \approx \frac{1}{2} \left(\frac{At_1}{\ln(1.3)} + \frac{At_2}{\ln(1.5)} \right) \Rightarrow \sigma_3 \approx 8.75 - 96.12 \times \sigma_4.$$

Note that we must choose $\sigma_4 < 0.0911$ in order to have $\sigma_3 > 0$. Taking for instance $\sigma_4 = 0.01$, we have consequently also $\sigma_3 = 7.79$.

A.7. P -equation.

Basal PNC growth rate r_P . In [16, Table I] it is reported that the mean total neurite length/neuron after $2^{3/4}$ hours in conditioned medium was $408 \text{ } \mu\text{m}$, while in the unconditioned medium it was $118 \text{ } \mu\text{m}$ (they study ciliary ganglia, which are parasympathetic ganglia located in the posterior orbit). Taking the latter as the initial value P_0 , we have from the equation describing PNC dynamics in this context

$$\begin{aligned} P(t = 2^{3/4}\text{h} = 0.1146\text{day}) &= P_0 \exp(r_P \times t) \\ \Rightarrow 0.1146 \times r_P &= \ln \left(\frac{408}{118} \right) \\ \Rightarrow r_P &= 10.83 \text{ day}^{-1}. \end{aligned}$$

In the same reference we find another useful dataset in [16, Table II]. Here it is stated that the mean elongation rate of 14 neurites (chosen to be at least $15 \text{ } \mu\text{m}$ long) without any medium change was $22 \text{ } \mu\text{m/hour}$. Converting these lengths into cell numbers (using the calculations done in A.1) and keeping in mind that $1 \text{ hour} = 0.0417 \text{ days}$, we calculate the growth rate “per cell” r_P as $22/14 \times 15 \times 1/0.0417 = 2.51 \text{ day}^{-1}$.

Another way to determine r_P could be to use the data in [17, Table 1]. Here the authors measure the maximal effect on ciliary (parasympathetic) and sympathetic neurite growth in various culture media after 2 hours. Considering the data regarding the “standard” conditioned medium, we have that the relative neurite length for ciliary neurons was 3.42, and for sympathetic neurons 1.81. Then, assuming an exponential growth for both cell cultures, we have that $P_0 \exp(r_P t)/S_0 \exp(r_S t) = 3.42/1.81$; furthermore, taking $P_0 = S_0$ and

$t = 2\text{h} = 0.0833\text{day}$, we have that $r_P - r_S = 7.63 \text{ day}^{-1}$. Now, recalling our previous estimate for r_S ($r_S = 0.06$, see A.6), we have $r_P = 7.70 \text{ day}^{-1}$.

It is encouraging to see that all these three values are of the same order of magnitude. To choose an estimate for r_P , we take their average 7 day^{-1} .

PNC carrying capacity k_P . In absence of tumor, we know that the PNC equilibrium value is $P^{eq} = 0.026 \text{ cells/mm}^3$ (see section A.2). We then take $k_P = P^{eq}$.

NGF-enhanced PNC growth π_1, π_2 . [17] investigated (in vitro) the effect of NGF on promoting the parasympathetic ciliary ganglion outgrowth. Their calculations were used to calculate the mean total length of neurites per neuron. Their calculations were based on data from neurons that had at least one neurite greater than $15 \mu\text{m}$ in length (\approx about the diameter of the neuronal soma). In this regard when they added NGF to dissociate ciliary ganglion neurons, resulted in a 2-fold increase in neurite length over untreated, control cultures. They estimated the mean total neurite length per neuron for control cultures to be $79 \pm 19 \mu\text{m}$. Parasympathetic ganglion neurons were exposed to a concentration of $10\text{ng/mL} = \frac{10 \times 10^3}{10^3} \frac{\text{pg}}{\text{mm}^3}$ per h. Just two hours after addition of NGF the ratio $\frac{P_{NGF}}{P_{control}} \approx 2.08 \pm 0.12$.

Recalling the given P equation:

$$\frac{dP}{dt} = \left(r_P + \frac{G}{\pi_1 + \pi_2 G} \right) S \xrightarrow{G \text{ const}} P(t) = P_0 \exp \left[\left(r_P + \frac{G}{\pi_1 + \pi_2 G} \right) t \right] ;$$

so after two hours we have

$$\frac{P_{NGF}}{P_{control}} = \exp \left(\frac{G}{\pi_1 + \pi_2 G} \times \frac{2}{24} \right) = 2.08 .$$

Taking into account that $2 \text{ hours} \approx \frac{2}{24} \text{ day} = 0.083 \text{ day}$ we deduce that

$$\frac{10}{\pi_1 + \pi_2 \times 10} \times 0.083 = \ln 2.08$$

and therefore $\pi_1 = 1.33 - 10 \times \pi_2$. Note that it must be $\pi_2 < 0.13$ in order to have $\pi_1 > 0$. We can take for example $\pi_2 = 0.1$ and thus $\pi_1 = 0.33$.

A.8. N_n -equation.

Noradrenaline production by SNC s_n . Regarding the norepinephrine release rate, [31] estimated the apparent norepinephrine release rate at rest to be $0.54 \pm 0.20 \mu\text{g}/(\text{m}^2 \text{min}) = 777.60 \text{ pg}/\text{mm}^2 \times \text{day}$. Note that 90% of this release rate is due to the sympathetic nerves. To convert the mm^2 in cells, we assume once again a nerve cell radius $r = 13.5 \mu\text{m} = 13.5 \times 10^{-3} \text{m}$ (see A.1); the surface area is given by $4\pi r^2 = 4\pi(13.5 \times$

$10^{-3})^2 \approx 2.29 \times 10^{-3} \text{mm}^2$, thus we deduce that in 1mm^2 there are $1/(2.29 \times 10^{-3}) = 436.7$ nerve cells. The noradrenaline secretion rate is then given by $s_n = 0.9 \times 777.60/436.7 \approx 1.6 \text{ pg cells}^{-1} \text{day}^{-1}$.

Noradrenaline decay rate d_n . In [82] the noradrenaline half-life is reported to be about 10 hours (although this value is different in different tissues). This leads to a decay rate $d_n = 1.66 \text{ day}^{-1}$.

Noradrenaline uptake rate (by tumor cells) γ_5 . In [40, Figure 4A] we find one set of measurements of NE uptake by human pheochromocytoma⁸ cells. Recalling the molecular weight of NE found in A.1 and assuming a culture volume of 1 mL (it is not better specified in the paper), we can convert the datapoints in [40, Figure 4A] into our units and fit the function $N(t) = N_0 - N_0 \exp(-\gamma_5 T t)$ to them; note that T represents the tumor cells, and that the value of this function at each time t is measured as the initial substrate concentration minus the uptaken NE. Using the MatLab function `nlinfit` to fit the data gives:

```
>> jaques.substr = 169.18.*[1 2 3 4 5]
>> jaques.uptake = 169.18*10^(-3).*[15 32 45 53 65]
>> NEinternFIT(jaques)
Estimated gamma5 value = 0.0019926
ci for gamma5 =      0.0018      0.0022
```

The plot of the fit is reported in Figure 9.

Noradrenaline constant source c_n . We found in A.2 that in normal conditions (i.e. in the absence of a tumor) the level of noradrenaline is $N_n^{eq} = 300 \text{ pg/mm}^3$. We can then calculate c_n from the equilibrium equation

$$c_n + s_n S^{eq} - d_n N_n^{eq} = 0 \quad \Rightarrow \quad c_n \approx 500 \frac{\text{pg}}{\text{mm}^3 \text{day}},$$

where S^{eq} and P^{eq} were also found in A.2 and s_n, d_n were estimated above.

A.9. N_a -equation.

Acetylcholine release rate s_a . In [67] the output of acetylcholine from the plexus of the guinea-pig ileum longitudinal strip is used to study the mechanism of acetylcholine release. The resting output is reasonably constant for a given preparation for long periods; the mean value for eighty-four experiments was about $51 \text{ ng/g} \cdot \text{min}$. The evoked output, however, usually changes as stimulation is prolonged, in a manner varying with the stimulation used. Assuming a nerve cell volume of 10^{-5} mm^3 (see A.1) and of density equal to water's one (1g/mL), we

⁸A pheochromocytoma is a neuroendocrine tumor of the medulla of the adrenal glands; it secretes high amounts of catecholamines, mostly norepinephrine, plus epinephrine to a lesser extent.

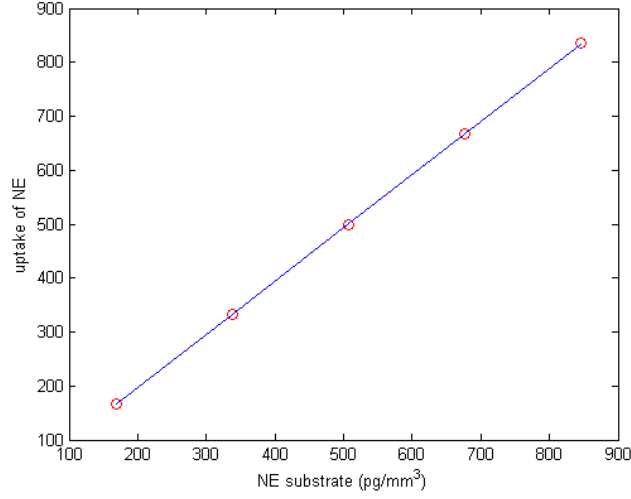


FIGURE 9. Plotting the data from [40] (red circles) together with the function $N(t) = N_0 - N_0 \exp(-\gamma_5 T t)$ (blue line) fitted to the data with the MatLab function `nlinfit`.

have that 1 g of parasympathetic nerves corresponds to approximately 10^8 cells. Therefore, we estimate the acetylcholine production rate as $s_a = 0.73 \text{ Pg/cell day}$.

Acetylcholine decay rate d_a . In [6] the authors studied the influence of the stimulus interval and the effect of Mn ions on facilitation⁹ of acetylcholine (ACh) release from parasympathetic nerve terminals in quiescent guinea-pig auricles. Here we also find that when conditioning trains of stimuli were applied, a second much longer lasting component of facilitation was found ($t_{1/2} \approx 4 \text{ s}$). Also, the decay to the control level displays a half time of about 20 min and can also be accelerated by frequent stimulation of the parasympathetic nerve fibres. In this regard we can estimate $d_a = 49.91 \text{ day}^{-1}$ (taking 20 min).

Acetylcholine constant source c_a . In A.2 we estimated that in normal conditions (i.e. in the absence of a tumor) the acetylcholine level in the tissue is $N_a^{eq} = 530 \text{ pg/mm}^3$. We can then calculate c_a from the equilibrium equation

$$c_a + s_a P^{eq} - d_a N_a^{eq} = 0 \quad \Rightarrow \quad c_a \approx 26.5 \times 10^3 \frac{\text{Pg}}{\text{mm}^3 \text{day}},$$

where S^{eq} and P^{eq} were also found in A.2 and s_a, d_a were estimated above.

⁹NOTE: Here the term *facilitation* denotes an increase in transmitter release during repetitive nerve excitation

REFERENCES

- [1] M. H. Antoni, S. K. Lutgendorf, S. W. Cole, F. S. Dhabhar, S. E. Sephton, P. G. McDonald, M. Stefanek, and A. K. Sood, *The influence of bio-behavioural factors on tumour biology: pathways and mechanisms*, Nat. Rev. Cancer **6** (2006), no. 3, 240–248.
- [2] G. E. Ayala, H. Dai, M. Powell, R. Li, Y. Ding, T. M. Wheeler, D. Shine, D. Kadmon, T. Thompson, B. J. Miles, M. M. Ittmann, and D. Rowley, *Cancer-related axonogenesis and neurogenesis in prostate cancer*, Clin. Cancer Res. **14** (2008), no. 23, 7593–7603.
- [3] M. E. Baker, *Molecular weight and structure of 7 S nerve growth factor protein*, J. Biol. Chem. **250** (1975), no. 5, 1714–1717.
- [4] F. Balkwill and A. Mantovani, *Inflammation and cancer: back to Virchow?*, THE LANCET **357** (2001), 539–545.
- [5] A. M. Ballangrud, W. H. Yang, A. Dnistrian, N. M. Lampen, and G. Sgouros, *Growth and characterization of LNCaP prostate cancer cell spheroids*, Clin. Cancer Res. **5** (1999), no. 10 Suppl, 3171s–3176s.
- [6] M. Bechem, H. G. Glitsch, and L. Pott, *Facilitation of acetylcholine release from cardiac parasympathetic nerve endings effect of stimulation pattern and mn ions*, Pflügers Archiv European Journal of Physiology **391** (1981).
- [7] V. Blanc, J. Nariculam, P. Munson, A. Freeman, H. Klocker, J. Masters, and M. Williamson, *A role for class 3 semaphorins in prostate cancer*, Prostate **71** (2011), no. 6, 649–658.
- [8] L. Capparuccia and L. Tamagnone, *Semaphorin signaling in cancer cells and in cells of the tumor microenvironment—two sides of a coin*, J. Cell. Sci. **122** (2009), no. Pt 11, 1723–1736.
- [9] P. Carmeliet and M. Tessier-Lavigne, *Common mechanisms of nerve and blood vessel wiring*, Nature **436** (2005), 193–200.
- [10] E. Castro-Rivera, S. Ran, P. Thorpe, and J. D. Minna, *Semaphorin 3B (SEMA3B) induces apoptosis in lung and breast cancer, whereas VEGF165 antagonizes this effect*, Proc. Natl. Acad. Sci. U.S.A. **101** (2004), no. 31, 11432–11437.
- [11] A. Chédotal, G. Kerjan, and C. Moreau-Fauvarque, *The brain within the tumor: new roles for axon guidance molecules in cancers*, Cell Death and Differentiation **12** (2005), 1044–1056.
- [12] C. F. Chiang, E. L. Son, and G. J. Wu, *Oral treatment of the TRAMP mice with doxazosin suppresses prostate tumor growth and metastasis*, Prostate **64** (2005), no. 4, 408–418.
- [13] Y. Chida, M. Hamer, J. Wardle, and A. Steptoe, *Do stress-related psychosocial factors contribute to cancer incidence and survival?*, Nat Clin Pract Oncol **5** (2008), no. 8, 466–475.
- [14] P. Claude, E. Hawrot, D. A. Dunis, and R. B. Campenot, *Binding, internalization, and retrograde transport of 125I-nerve growth factor in cultured rat sympathetic neurons*, J. Neurosci. **2** (1982), no. 4, 431–442.
- [15] S. W. Cole and A. K. Sood, *Molecular pathways: beta-adrenergic signaling in cancer*, Clin. Cancer Res. **18** (2012), no. 5, 1201–1206.
- [16] F. Collins and A. Dawson, *Conditioned medium increases the rate of neurite elongation: separation of this activity from the substratum-bound inducer of neurite outgrowth*, J. Neurosci. **2** (1982), no. 8, 1005–1010.
- [17] ———, *An effect of nerve growth factor on parasympathetic neurite outgrowth*, Proc. Natl. Acad. Sci. U.S.A. **80** (1983), no. 7, 2091–2094.
- [18] G. Dachille, T. Cai, G. M. Ludovico, G. Vestita, G. Pagliarulo, G. Nesi, S. Mazzoli, F. Meacci, N. Mondaini, B. Detti, and R. Bartoletti, *Prognostic role of*

- cell apoptotic rate in prostate cancer: outcome of a long-time follow-up study*, *Oncol. Rep.* **19** (2008), no. 2, 541–545.
- [19] B. Dickson, *Molecular mechanisms of axon guidance*, *Science* **298** (2003), 1959–1964.
 - [20] L. Dolle, I. El Yazidi-Belkoura, E. Adriaenssens, V. Nurcombe, and H. Hondermarck, *Nerve growth factor overexpression and autocrine loop in breast cancer cells*, *Oncogene* **22** (2003), no. 36, 5592–5601.
 - [21] L. Dollé, M. Oliveira, E. Bruyneel, H. Hondermarck, and M. Bracke, *Nerve growth factor mediates its pro-invasive effect in parallel with the release of a soluble E-cadherin fragment from breast cancer MCF-7/AZ cells*, *Journal of Dairy Research* **72** (2005), no. Special Issue, 20–26.
 - [22] T. Drell IV, J. Joseph, K. Lang, B. Niggemann, K. Zaenker, and F. Entschladen, *Effects of neurotransmitters on the chemokinesis and chemotaxis of MDA-MB-468 human breast carcinoma cells*, *Breast Cancer Research and Treatment* **80** (2003), 63–70.
 - [23] P. B. Ehrhard, P. Erb, U. Graumann, and U. Otten, *Expression of nerve growth factor and nerve growth factor receptor tyrosine kinase Trk in activated CD4-positive T-cell clones*, *Proc. Natl. Acad. Sci. U.S.A.* **90** (1993), no. 23, 10984–10988.
 - [24] A. Eichmann, T. Makinen, and K. Alitalo, *Neural guidance molecules regulate vascular remodeling and vessel navigation*, *Genes & Development* **19** (2005), 1013–1021.
 - [25] J. W. Eng, K. M. Kokolus, C. B. Reed, B. L. Hylander, W. W. Ma, and E. A. Repasky, *A nervous tumor microenvironment: the impact of adrenergic stress on cancer cells, immunosuppression, and immunotherapeutic response*, *Cancer Immunol. Immunother.* **63** (2014), no. 11, 1115–1128.
 - [26] F. Entschladen, T. Drell IV, K. Lang, J. Joseph, and K. Zaenker, *Tumor-cell migration, invasion, and metastasis: navigation by neurotransmitters*, *Lancet Oncol* **5** (2004), 254–258.
 - [27] F. Entschladen, K. Lang, T. Drell, J. Joseph, and K. Zaenker, *Neurotransmitters are regulators for the migration of tumor cells and leukocytes*, *Cancer Immunol Immunother* **51** (2002), 467–482.
 - [28] F. Entschladen, D. Palm, K. Drell IV, T. Lang, and K. Zaenker, *Connecting a tumor to the environment*, *Current Pharmaceutical Design* **13** (2007), no. 33, 3440–3444.
 - [29] F. Entschladen, D. Palm, K. Lang, T. Drell IV, and K. Zaenker, *Neoneurogenesis: Tumors may initiate their own innervation by the release of neurotrophic factors in analogy to lymphangiogenesis and neoangiogenesis*, *Medical Hypotheses* **67** (2006), 33–35.
 - [30] F. Entschladen, D. Palm, B. Niggemann, and K. Zaenker, *The cancer’s nervous tooth: Considering the neuronal crosstalk within tumors*, *Seminars in Cancer Biology* **18** (2008), 171–175.
 - [31] M. Esler, G. Jackman, A. Bobik, D. Kelleher, G. Jennings, P. Leonard, H. Skews, and P. Korner, *Determination of norepinephrine apparent release rate and clearance in humans*, *Life Sciences* **25** (1979), 1461–1470.
 - [32] J. C. Fiala and K. M. Harris, *Dendrite structure*, *Dendrites* (1999).
 - [33] I. J. Fidler and S. Paget, *The pathogenesis of cancer metastasis: the ‘seed and soil’ hypothesis revisited*, *Nat. Rev. Cancer* **3** (2003), no. 6, 453–458.
 - [34] R. L. Friede, *The relationship of body size, nerve cell size, axon length, and glial density in the cerebellum*, *Proc. Natl. Acad. Sci. U.S.A.* **49** (1963), 187–193.
 - [35] A. Geldof, E. van Haarst, and D. Newling, *Neurotrophic factors in prostate and prostatic cancer*, *Prostate Cancer and Prostatic Diseases* **5** (1998), 236–241.

- [36] L. S. Goodman and A. Gilman, *Goodman & Gilman's pharmacological basis of therapeutics, chapter 8*, 12th ed., 2011.
- [37] A. C. Guyton and J. E. Hall, *Textbook of medical physiology, chapter 60*, 11th ed., 2006.
- [38] J. G. Herman and G. G. Meadows, *Increased class 3 semaphorin expression modulates the invasive and adhesive properties of prostate cancer cells*, *Int. J. Oncol.* **30** (2007), no. 5, 1231–1238.
- [39] Y. Jaimes, C. Gras, L. Goudeva, S. Buchholz, B. Eiz-Vesper, A. Seltsam, S. Immenschuh, R. Blasczyk, and C. Figueiredo, *Semaphorin 7A inhibits platelet production from CD34+ progenitor cells*, *J. Thromb. Haemost.* **10** (2012), no. 6, 1100–1108.
- [40] S. Jaques, M. C. Tobes, and J. C. Sisson, *Sodium dependency of uptake of norepinephrine and m-iodobenzylguanidine into cultured human pheochromocytoma cells: evidence for uptake-one*, *Cancer Res.* **47** (1987), no. 15, 3920–3928.
- [41] K. Keino-Masu, M. Masu, L. Hinck, E. D. Leonardo, S. S. Chan, J. G. Culotti, and M. Tessier-Lavigne, *Deleted in Colorectal Cancer (DCC) encodes a netrin receptor*, *Cell* **87** (1996), no. 2, 175–185.
- [42] B. Kigel, A. Varshavsky, O. Kessler, and G. Neufeld, *Successful inhibition of tumor development by specific class-3 semaphorins is associated with expression of appropriate semaphorin receptors by tumor cells*, *PLoS ONE* **3** (2008), no. 9, e3287.
- [43] K. S. Korolev, J. B. Xavier, and J. Gore, *Turning ecology and evolution against cancer*, *Nature Reviews Cancer* **14** (2014), no. 5, 371–380.
- [44] M. S. Kuzirian, A. R. Moore, E. K. Staudenmaier, R. H. Friedel, and S. Paradis, *The class 4 semaphorin Sema4D promotes the rapid assembly of GABAergic synapses in rodent hippocampus*, *J. Neurosci.* **33** (2013), no. 21, 8961–8973.
- [45] R. Kvetnansky, K. Pacak, K. Fukuhara, E. Viskupic, B. Hiremagalur, B. Nankova, D. S. Goldstein, E. L. Sabban, and I. J. Kopin, *Sympathoadrenal system in stress. Interaction with the hypothalamic-pituitary-adrenocortical system*, *Ann. N. Y. Acad. Sci.* **771** (1995), 131–158.
- [46] K. Lang and P. Bastian, *Neurotransmitter effects on tumor cells and leukocytes*, *Prog Exp Tumor Res. Basel, Karger* **39** (2007), 99–121.
- [47] K. Lang, T. Drell IV, B. Niggemann, K. Zänker, and F. Entschladen, *Neurotransmitters regulate the migration and cytotoxicity in natural killer cells*, *Immunology Letters* **90** (2003), 165–172.
- [48] A. Latil, L. Chêne, B. Cochant-Priollet, P. Mangin, G. Fournier, P. Berthon, and O. Cussenot, *Quantification of expression of netrins, slits and their receptors in human prostate tumors*, *Int. J. Cancer* **103** (2003), 306–315.
- [49] R. M. Lindsay, *Nerve growth factors (NGF, BDNF) enhance axonal regeneration but are not required for survival of adult sensory neurons*, *J. Neurosci.* **8** (1988), no. 7, 2394–2405.
- [50] L. Liotta, *An attractive force in metastasis*, *Nature* **410** (2001), 24–25.
- [51] S. Lü, Y. Zhou, H. Que, and S. Liu, *Peptidergic innervation of human esophageal and cardiac carcinoma*, *World J Gastroenterol* **9** (2003), no. 3, 399–403.
- [52] S. K. Lutgendorf, K. DeGeest, L. Dahmouch, D. Farley, F. Penedo, D. Bender, M. Goodheart, T. E. Buekers, L. Mendez, G. Krueger, L. Clevenger, D. M. Lubaroff, A. K. Sood, and S. W. Cole, *Social isolation is associated with elevated tumor norepinephrine in ovarian carcinoma patients*, *Brain Behav. Immun.* **25** (2011), no. 2, 250–255.

- [53] S. Madduri, M. Papaloizos, and B. Gander, *Synergistic effect of GDNF and NGF on axonal branching and elongation in vitro*, *Neurosci. Res.* **65** (2009), no. 1, 88–97.
- [54] C. Magnon, S. Hall, J. Lin, X. Xue, L. Gerber, S. Freedland, and P. Frenette, *Autonomic nerve development contributes to prostate cancer progression*, *Science* **341** (2013), 1236361.
- [55] C. Manitt, M. A. Colicos, K. M. Thompson, E. Rousselle, A. C. Peterson, and T. E. Kennedy, *Widespread expression of netrin-1 by neurons and oligodendrocytes in the adult mammalian spinal cord*, *J. Neurosci.* **21** (2001), no. 11, 3911–3922.
- [56] P. Mehlen, C. Delloye-Bourgeois, and A. Chedotal, *Novel roles for Slits and netrins: axon guidance cues as anticancer targets?*, *Nat. Rev. Cancer* **11** (2011), no. 3, 188–197.
- [57] L. E. Miller, H. P. Justen, J. Scholmerich, and R. H. Straub, *The loss of sympathetic nerve fibers in the synovial tissue of patients with rheumatoid arthritis is accompanied by increased norepinephrine release from synovial macrophages*, *FASEB J.* **14** (2000), no. 13, 2097–2107.
- [58] M. Moreno-Smith, S. K. Lutgendorf, and A. K. Sood, *Impact of stress on cancer metastasis*, *Future Oncol* **6** (2010), no. 12, 1863–1881.
- [59] B. Mravec, Y. Gidron, and I. Hulin, *Neurobiology of cancer: Interactions between nervous, endocrine and immune systems as a base for monitoring and modulating the tumorigenesis by the brain*, *Seminars in Cancer Biology* **18** (2008), 150–163.
- [60] R. A. Murphy, J. D. Saide, M. H. Blanchard, and M. Young, *Molecular properties of the nerve growth factor secreted in mouse saliva*, *Proc. Natl. Acad. Sci. U.S.A.* **74** (1977), no. 7, 2672–2676.
- [61] A. L. Nagler, W. D. Dettbarn, and S. M. Levenson, *Tissue levels of acetylcholine and acetylcholinesterase weanling germfree rats subjected to acute choline deficiency*, *J. Nutr.* **95** (1968), no. 4, 603–606.
- [62] J. C. Nickel, *Benign prostatic hyperplasia: does prostate size matter?*, *Rev Urol* **5 Suppl 4** (2003), S12–17.
- [63] K. Ondicova and B. Mravec, *Role of nervous system in cancer aetiopathogenesis*, *Lancet Oncol* **11** (2010), 596–601.
- [64] K. Pacak, M. Palkovits, R. Kvetnansky, G. Yadid, I. J. Kopin, and D. S. Goldstein, *Effects of various stressors on in vivo norepinephrine release in the hypothalamic paraventricular nucleus and on the pituitary-adrenocortical axis*, *Ann. N. Y. Acad. Sci.* **771** (1995), 115–130.
- [65] D. Palm and F. Entschladen, *Neoneurogenesis and the neuro-neoplastic synapse*, *Prog Exp Tumor Res. Basel, Karger* **39** (2007), 91–98.
- [66] S. Park, R. R. Ang, S. P. Duffy, J. Bazov, K. N. Chi, P. C. Black, and H. Ma, *Morphological differences between circulating tumor cells from prostate cancer patients and cultured prostate cancer cells*, *PLoS ONE* **9** (2014), no. 1, e85264.
- [67] W. D. Paton, E. S. Vizi, and M. A. Zar, *The mechanism of acetylcholine release from parasympathetic nerves*, *J. Physiol. (Lond.)* **215** (1971), no. 3, 819–848.
- [68] K. J. Pienta, N. McGregor, R. Axelrod, and D. E. Axelrod, *Ecological therapy for cancer: defining tumors using an ecosystem paradigm suggests new opportunities for novel cancer treatments*, *Transl Oncol* **1** (2008), no. 4, 158–164.
- [69] K. J. Pienta, H. Naik, A. Akhtar, K. Yamazaki, T. S. Replogle, J. Lehr, T. L. Donat, L. Tait, V. Hogan, and A. Raz, *Inhibition of spontaneous metastasis in a rat prostate cancer model by oral administration of modified citrus pectin*, *J. Natl. Cancer Inst.* **87** (1995), no. 5, 348–353.

- [70] J. F. Poduslo and G. L. Curran, *Permeability at the blood-brain and blood-nerve barriers of the neurotrophic factors: NGF, CNTF, NT-3, BDNF*, Brain Res. Mol. Brain Res. **36** (1996), no. 2, 280–286.
- [71] E. M. Rakowicz-Szulczynska, *Identification of the cell surface and nuclear receptors for NGF in a breast carcinoma cell line*, J. Cell. Physiol. **154** (1993), no. 1, 64–70.
- [72] G. Ramesh, A. Berg, and C. Jayakumar, *Plasma netrin-1 is a diagnostic biomarker of human cancers*, Biomarkers **16** (2011), no. 2, 172–180.
- [73] A. Ricci, S. Greco, S. Mariotta, L. Felici, E. Bronzetti, A. Cavazzana, G. Cardillo, F. Amenta, A. Bisetti, and G. Barbolini, *Neurotrophins and neurotrophin receptors in human lung cancer*, Am. J. Respir. Cell Mol. Biol. **25** (2001), 439–446.
- [74] K. G. Ruit, P. A. Osborne, R. E. Schmidt, E. M. Johnson, and W. D. Snider, *Nerve growth factor regulates sympathetic ganglion cell morphology and survival in the adult mouse*, J. Neurosci. **10** (1990), no. 7, 2412–2419.
- [75] H. P. Schmid, J. E. McNeal, and T. A. Stamey, *Observations on the doubling time of prostate cancer. The use of serial prostate-specific antigen in patients with untreated disease as a measure of increasing cancer volume*, Cancer **71** (1993), no. 6, 2031–2040.
- [76] J. S. Schuman, T. Pedut-Kloizman, E. Hertzmark, M. R. Hee, J. R. Wilkins, J. G. Coker, C. A. Puliafito, J. G. Fujimoto, and E. A. Swanson, *Reproducibility of nerve fiber layer thickness measurements using optical coherence tomography*, Ophthalmology **103** (1996), no. 11, 1889–1898.
- [77] L. V. Sharova, A. A. Sharov, T. Nedorezov, Y. Piao, N. Shaik, and M. S. Ko, *Database for mRNA half-life of 19 977 genes obtained by DNA microarray analysis of pluripotent and differentiating mouse embryonic stem cells*, DNA Res. **16** (2009), no. 1, 45–58.
- [78] A. K. Sood, G. N. Armaiz-Pena, J. Halder, A. M. Nick, R. L. Stone, W. Hu, A. R. Carroll, W. A. Spannuth, M. T. Deavers, J. K. Allen, L. Y. Han, A. A. Kamat, M. M. Shahzad, B. W. McIntyre, C. M. Diaz-Montero, N. B. Jennings, Y. G. Lin, W. M. Merritt, K. DeGeest, P. E. Vivas-Mejia, G. Lopez-Berestein, M. D. Schaller, S. W. Cole, and S. K. Lutgendorf, *Adrenergic modulation of focal adhesion kinase protects human ovarian cancer cells from anoikis*, J. Clin. Invest. **120** (2010), no. 5, 1515–1523.
- [79] W. D. Stein, W. D. Figg, W. Dahut, A. D. Stein, M. B. Hoshen, D. Price, S. E. Bates, and T. Fojo, *Tumor growth rates derived from data for patients in a clinical trial correlate strongly with patient survival: A novel strategy for evaluation of clinical trial data*, The Oncologist **13** (2008), 1046–1054.
- [80] K. Syrigos, *Prostate cancer: Biology, diagnosis and management*, Oxford University Press, USA, 2001.
- [81] B. Tang, M. Wang, and B. Wise, *Nerve growth factor mRNA stability is controlled by a cis-acting instability determinant in the 3'-untranslated region*, Brain Res Mol Brain Res. **46** (1997), no. 1-2, 118–126.
- [82] H. L. Taubin, B. Djahanguiri, and L. Landsberg, *Noradrenaline concentration and turnover in different regions of the gastrointestinal tract of the rat: an approach to the evaluation of sympathetic activity in the gut*, Gut **13** (1972), no. 10, 790–795.
- [83] P. H. Thaker and A. K. Sood, *Neuroendocrine influences on cancer biology*, Semin. Cancer Biol. **18** (2008), no. 3, 164–170.
- [84] K. Thiébault, L. Mazelin, L. Pays, F. Llambi, M. Joly, J. Scoazec, J. Saurin, G. Romeo, and P. Mehlen, *The netrin-1 receptors UNC5H are putative tumor*

- suppressors controlling cell death commitment*, PNAS **100** (2003), no. 7, 4173–4178.
- [85] J. H. University, *Animal care and use committee – the mouse*.
 - [86] A. Villers, J. McNeal, E. Redwine, F. Freiha, and T. Stamey, *The role of perineural space invasion in the local spread of prostatic adenocarcinoma*, The Journal of Urology **142** (1989), no. 3, 763–768.
 - [87] E. Vissoci Reiche, S. Odebrecht Vargas Nunes, and H. Kaminami Morimoto, *Stress, depression, the immune system, and cancer*, THE LANCET Oncology **5** (2004), 617–625.
 - [88] K. H. Wang, K. Brose, D. Arnott, T. Kidd, C. S. Goodman, W. Henzel, and M. Tessier-Lavigne, *Biochemical purification of a mammalian slit protein as a positive regulator of sensory axon elongation and branching*, Cell **96** (1999), no. 6, 771–784.
 - [89] T. Watanabe, M. Inoue, K. Sasaki, M. Araki, S. Uehara, K. Monden, T. Saika, Y. Nasu, H. Kumon, and M. B. Chancellor, *Nerve growth factor level in the prostatic fluid of patients with chronic prostatitis/chronic pelvic pain syndrome is correlated with symptom severity and response to treatment*, BJU Int. **108** (2010), no. 2, 248–251.
 - [90] I. Wessler and C. J. Kirkpatrick, *Acetylcholine beyond neurons: the non-neuronal cholinergic system in humans*, Br. J. Pharmacol. **154** (2008), no. 8, 1558–1571.
 - [91] C. J. Woolf, B. Safieh-Garabedian, Q. P. Ma, P. Crilly, and J. Winter, *Nerve growth factor contributes to the generation of inflammatory sensory hypersensitivity*, Neuroscience **62** (1994), no. 2, 327–331.
 - [92] Y. Xu, L. Yuan, J. Mak, L. Pardanaud, M. Caunt, I. Kasman, B. Larrivee, R. Del Toro, S. Suchting, A. Medvinsky, J. Silva, J. Yang, J. L. Thomas, A. W. Koch, K. Alitalo, A. Eichmann, and A. Bagri, *Neuropilin-2 mediates VEGF-C-induced lymphatic sprouting together with VEGFR3*, J. Cell Biol. **188** (2010), no. 1, 115–130.
 - [93] Z. W. Zhu, H. Friess, L. Wang, T. Bogardus, M. Korc, J. Kleeff, and M. W. Buchler, *Nerve growth factor exerts differential effects on the growth of human pancreatic cancer cells*, Clin. Cancer Res. **7** (2001), no. 1, 105–112.

CONTENTS

Significance Statement	2
1. Introduction	3
2. Biological background	3
2.1. Neurons, neurotransmitters and the Autonomic Nervous System (ANS)	3
2.2. Tumor-induced neoneurogenesis	4
2.3. ANS effects on tumor progression	4
3. Mathematical model	5
3.1. Model equations	6
3.2. Parameters and initial conditions	9
4. Results	9
4.1. PSA	12
4.2. Stress and tumor progression	12
4.3. Blocking tumor acetylcholine receptors	14
5. Discussion	14
Acknowledgment	15
Appendix A. Parameter estimation	15
A.1. Standard sizes and weights	15
A.2. Equilibrium values	16
A.3. T_p -equation	17
A.4. G -equation	21
A.5. A -equation	22
A.6. S -equation	24
A.7. P -equation	27
A.8. N_n -equation	28
A.9. N_a -equation	29
References	31